Small Satellite Electromagnetic Docking System

Modeling and Control

by

Aaditya Ravindran

A Thesis Presented in Partial Fulfillment
of the Requirements for the Degree
Master of Science

Approved April 2018 by the
Graduate Supervisory Committee:

Jekanthan Thangavelutham, Co-Chair
Hugh James Barnaby , Co-Chair
Md. Ashfaque Bin Shafique

ARIZONA STATE UNIVERSITY

May 2018

ABSTRACT

There is a growing need for interplanetary travel technology development. There are hence plans to build deep space human habitats, communication relays, and fuel depots. These can be classified as large space structures. To build large structures, it is essential that these are modular in nature. With modularization of structures, it becomes essential that interconnection of modules is developed. Docking systems enable interconnection of modules. The state-of-the-art technology in docking systems is the Power Data Grapple Fixture (PDGF), used on the International Space Station by the Canadarm2 robotic arm to grapple, latch onto and provide power to the object it has grappled. The PDGF is operated by highly skilled astronauts on the ISS and are prone to human errors. Therefore, there is a need for autonomous docking. Another issue with the PDGF is that it costs around 1 to 2 million US dollars to build the 26-inch diameter docking mechanism. Hence, there is a growing need to build a lower cost and scalable, smaller docking systems. Building scalable smaller docking systems will hence enable testing them on small satellites. With the increasing need for small, low cost, autonomous docking systems, this thesis has been proposed. This thesis focuses on modeling and autonomous control of an electromagnetic probe and cone docking mechanism. The electromagnetic docking system is known to be a highly nonlinear system. Hence, this work discusses various control strategies for this docking system using a levitation strategy.

ACKNOWLEDGMENTS

I would first like to thank my thesis advisor and mentor Dr. Jekanthan Thangavelutham, Assistant Professor, Department of Aerospace and Mechanical Engineering at the University of Arizona. I was fortunate to be guided by him both for my thesis as well as on other projects I took up under his guidance in the SpaceTREx laboratory. He has constantly motivated and steered me in the right direction whenever I needed it.

I would also like to extend my gratitude towards my co-chair Dr. Hugh James Barnaby, Assistant Professor, and Dr. Ashfaque Bin Shafique, Faculty Associate, Arizona State University for consenting to be on my thesis committee and reviewing my thesis.

I would also like to thank my fellow colleagues and current Ph.D. students at the SpaceTREx laboratory, Himangshu Kalita for his support and helping me in designing the simulation, Aman Chandra for guiding me in writing my thesis document, Ravi Teja Nallapu for his constant help and support.

TABLE OF CONTENTS

Page

CHAPTER Page

LIST OF TABLES

LIST OF FIGURES

Figure Page

Figure Page

Chapter 1

INTRODUCTION

Space was once a new frontier in human exploration. Development of technology took astronomy into space, with the deployment of the Hubble Space Telescope (Figure 1.1). The Hubble Space Telescope, around 13 meters long and around 4 meters wide had a defective primary mirror [2]. This is not the only problem it had [3]. The gyroscope, responsible for controlling the rotation of the spacecraft, to achieve pointing, was also defective. About six months later, the second out of the third gyro failed. There was also a memory failure in one of the flight computers. Thankfully, it was built to be serviced in space. Astronauts from the Endeavor space shuttle mission were able to rectify the mirror by adding corrective optics and add new gyros in multiple stages. The Hubble Space Telescope was finally able to take crisp images. The system was not perfect. As any other instruments, space structures have their own lifespan. To keep it going, it has been serviced at least five times to date. The Hubble Space Telescope is an example of the nature of human beings to explore the boundless. It has outlived its expected lifespan and is no longer expected to be serviced. The total telescope budget was around 4.7 billion USD, and it cost around 6 billion USD to service the spacecraft, totaling to about 10 billion USD for the whole project. Servicing and repair can hence be considered an important aspect of space technology development.

After the Hubble Telescope, the International Space Station (ISS) (Figure 1.2) was the next step towards space technology development. The ISS is probably the biggest structure assembled in space till date. The Russian module, Zarya, is the first module of the ISS, which was launched in November 1998. The first crew members

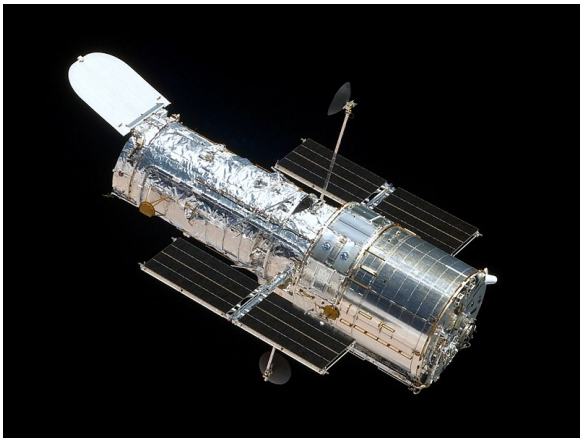

Figure 1.1: The Hubble Space Telescope

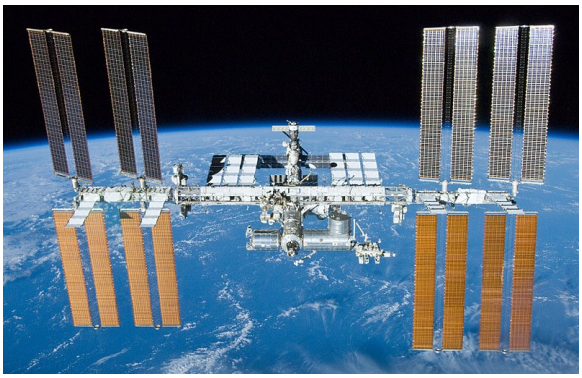

Figure 1.2: The International Space Station

reached the ISS in November 2000 [4]. Since then, it has been continually occupied by rotating crews, as a joint effort by the participant countries. As of March 2018, eighteen countries have been a part of the ISS project, for building, servicing as well as providing astronauts. It was deemed to be "complete" by 2011, but it continues to get new modules and components. Some key technologies which made this possible are in-space docking, docking mechanism designs, spacecraft modularity, and robotic assembly.

Space science research is moving towards colonizing the Moon and Mars. Before achieving colonization, it is essential that large structures are assembled in space like

the ISS. Large space structures not only facilitate colonization but also astronomy. The larger a telescope is, the larger is its light gathering capacity, and hence it can peer deeper into the depths of space and time. The amount of rocket fuel consumed by a rocket is directly linked to the weight of the payload. Larger spacecrafts require more fuel. To build big space structures it is essential that they are modular. Modularity will ensure that the structures could be assembled in space as well as repaired. Space structures would have to be repaired in order to last long if we want these structures deep in space.

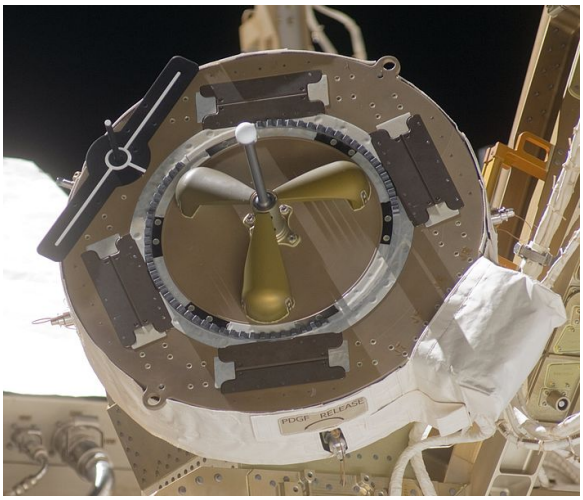

Figure 1.3: The Power Data Grapple Fixture

To assemble large structures in space and to repair, it is essential that efficient docking mechanisms are developed. Even though there are docking mechanisms like the docking mechanism of the ISS and the Power Data Grapple Fixture (PDGF), (Figure 1.3) of the robotic arms of the ISS, and the Soyuz docking system, these docking mechanisms are costly and have not been designed for small spacecrafts. Another major concern is that these are operated by astronauts and on June 25, 1997, during docking tests of manual control TORU, due to an astronaut error while docking, the Russian supply vehicle Progress 234 collided with the Mir space station,

rupturing it and nearly forcing the evacuation of the space station [5]. It is therefore essential that docking mechanisms are automated, removing humans from the loop, as even skilled astronauts are prone to errors and finding skilled astronauts is a concern.

Small satellites have revolutionized the space industry by enabling academic and private institutions to test mission concepts and technology, thereby providing valuable experience as well as advancing space technology. Small satellite docking mechanisms are still being ground tested and yet to be flown. With the growing popularity of small satellite docking, it is essential that different docking mechanisms are explored.

Docking mechanisms not only provide the capability of in-space assembly and repair, but also enable a myriad of applications swarm satellites can bring. For example, a swarm of satellites can be deployed and can dock together to perform data and power transfer. This can create a network of swarm satellites capable of resource sharing, including exchange of information, power, processing capability, sensor fusion to name a few. Docking systems could also enable small satellites to share information and sensors with bigger satellites. Small satellites would be able to repair faulty equipment in larger satellites and also provide redundancy to components about to reach their shelf life. This would drastically increase the performance and life time of a large satellite, thereby increasing the productivity vs. cost ratio or the value for money. This can not only help repair of components, but also used for reconnaissance on deep space missions. Small satellites could be deployed from large mothership satellites and these satellites could perform the necessary task, come back to the mothership, dock for both refueling and data power transfer, which can benefit both ways.

To enable these multiple applications of autonomous docking systems for small satellites, it is essential that this system is modularized so that this system can be used on multiple small satellites and also on large satellites. These modules can be

attached, detached and modified as docking technology for small satellites progresses. To fulfill this growing need for autonomous small satellite docking systems, this thesis has been presented.

1.1 Thesis Statement

The need for big space structures has driven the development in-space assembly and repair of spacecrafts. In-space assembly and repair are possible, primarily due to the docking mechanism. Docking of large spacecrafts has been demonstrated on numerous occasions with humans in the loop. The same is not true for small satellites. Hence, the development of an autonomous docking mechanism for nanosatellites is essential for the small satellite community. This thesis focuses on modeling and control of a general electromagnetic docking system for nanosatellites. Some key techniques in modeling an electromagnetic docking system and control of the docking system have been presented.

1.2 Thesis Document Organization

This document is organized into eight chapters. This chapter provided an introduction to the topic of in-orbit assembly, repair, and spacecraft docking, while motivating the thesis objective. First, applications of large space structures were discussed. Then, in-space assembly of these structures is discussed, followed by spacecraft docking. The idea was then modified to fit a small satellite. The motivation behind the end goal of data and power transfer was also discussed and concluded with the advantage of modularity of the docking mechanism. chapter 2 introduces the current technologies in the field of docking mechanisms. Docking system classification is presented followed by the ISS Docking system. Later, the current state of small spacecraft docking and related work in the field is discussed. Here, missions related

to the technology demonstration of docking mechanisms for small spacecrafts is discussed followed by research papers explaining various docking mechanisms. chapter 3 provides a detailed description of the design strategy of the thesis. The simulation of the system is presented followed by the design of the orbit propagator. The model of the docking system is explained in detail, followed by the design of the controllers for docking. The integration of the entire system follows this. With the system design completed, a mission concept, along with the mission and subsystem objectives are discussed in chapter 4. Results are discussed in chapter 5. Various graphs of the controller docking system are presented followed by the simulation figures. Some discussion explaining the results follows this. The document ends with the Conclusion and Future Work in chapter 6. A summary of the entire work is presented and concluded by a discussion on future hardware testing and possible mission proposals.

Chapter 2

CURRENT TECHNOLOGY AND RELATED WORK

2.1 Spacecraft Docking Mechanisms

Docking mechanisms for spacecrafts are can mainly be used for two purposes, berthing or data and power transfer. Docking mechanisms which are used for berthing can also provide data and power transfer, along with the main purpose of crew transfer. The docking systems developed for berthing the ISS are tested on big spacecrafts like for the Gemini, Apollo, Soyuz (Figure 2.1), [6]. Most docking systems which have been designed are probe and cone based systems. Probe and cone, also known as probe and drogue systems, consist of a probe, which will fit into a hollow cone. Other docking systems are considered a hybrid, like the Russian Hybrid interface mechanism [6, p. 20] which are also a modified version of the probe and cone docking mechanism.

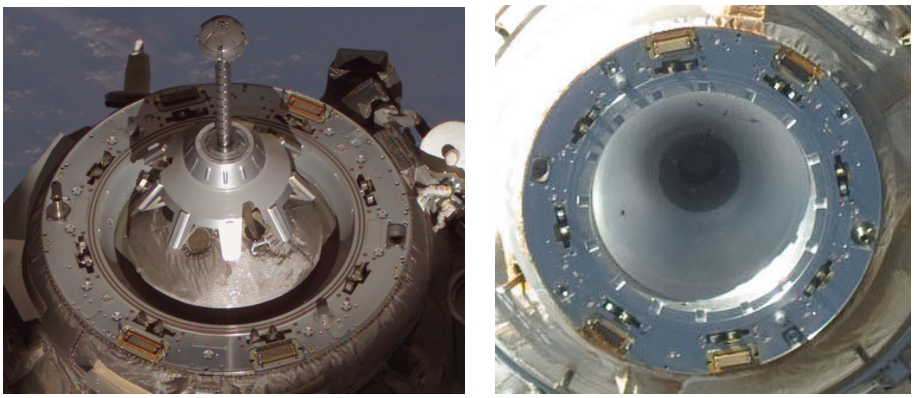

(a) Probe (b) Drogue

Figure 2.1: The Docking System of Soyuz

2.2 Current Status of Small Satellite Docking

Currently, docking systems have been tested extensively for big spacecrafts. Docking system designs have improved over the years, but largely remain the same. The same design strategy can be proposed for small satellites, but have yet to be proved in practice. Various designs for docking small satellites have been researched, but not tested. Cubesat missions for small satellite docking have been proposed, however have not been flown as of March 2018. The technology readiness level (TRL) for small satellite docking can be set at 4 or 5, indicating technology development and early stages of technology demonstration.

2.3 Cubesat Missions on Small Satellite Docking

Various cubesat missions for technology demonstration have been proposed. This section lists some of these missions.

2.3.1 AAReST Mission

Underwood et al. [7] have proposed a cubesat mission to demonstrate the concept of Autonomous Assembly of Reconfigurable Space Telescope (AAReST). The mission proposes a 15U cubesat which will demonstrate in-space assembly of the MirrorSats, Figure 2.2. To perform in-space assembly, the rendezvous and docking system has been designed as a probe and cone docking system with electromagnets and attitude control strategies for coarse docking, a Microsoft Kinect based array of sensors, LIDAR and Camera RDV sensors, a differential GPS for relative navigation. The authors have described tests that have been performed to dock the cubesats using the electromagnetic docking mechanism. According to Eckersley et al. [8], the AAReST mission is set to be launched in 2018 or later.

Figure 2.2: The AAReST Mission MirrorSats with Docking System

2.3.2 CPOD Mission

Bowen et al. [9] have proposed a Cubesat based rendezvous, Proximity Operations, and Docking (CPOD) mission, previously known as the Proximity Operations Nano-Satellite Flight Demonstrator, PONSFD [10] solely to test small satellite docking. They propose the use of a Universal Docking Port (UDP) [11], a semi-androgynous docking mechanism used in SPHERES [12]. The CPOD mission proposes 4 docking sensors in the Remote Proximity Operations and Docking (RPOD) module (Figure 2.3) which are, near and wide field visible range cameras and near and wide field IR cameras. This mission is said to demonstrate the capability of the UDP. According to the authors, the CPOD mission is also set to launch in 2018 or later.

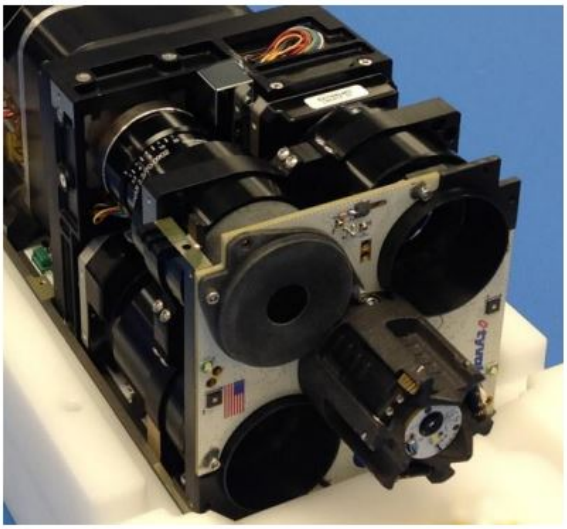

Figure 2.3: The CPOD Mission RPOD Module

2.3.3 ARCADE-R2 Mission

Barbetta et al. [13] have proposed an Autonomous Rendezvous, Control and Docking Experiment - Reflight 2 (ARCADE-R2). This mission was proposed as a technology demonstrator experiment to prove the feasibility of small satellite docking. On October 10, 2013, it flew on board the BEXUS-17 stratospheric balloon, successfully performing the docking procedures. The docking system (Figure 2.4) design is again a probe and cone based system with IR LEDs and IR LDR sensors to assist in the docking. The actuation was performed using the on-board attitude control system.

2.3.4 Permanent Magnet Docking System

Pei et al. [14] have proposed an autonomous rendezvous and docking system using permanent magnet docking mechanism. The mission acts as a technology demonstrator for a permanent magnet docking mechanism. The authors propose an attitude and position control using relative position navigation with the help of Continuous

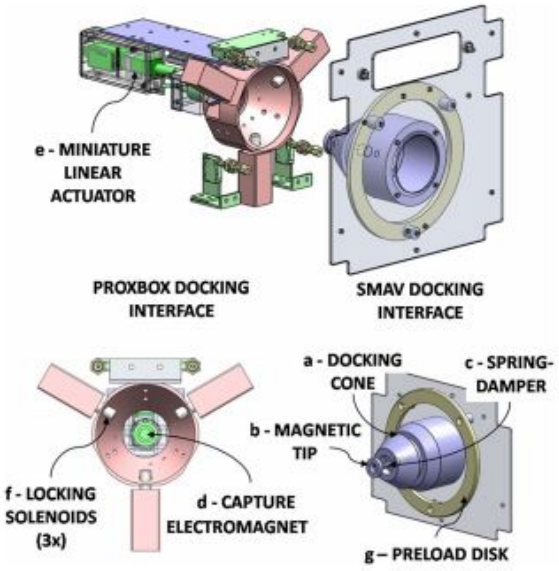

Figure 2.4: The ARCADE-R2 Mission Docking System

Differential GPS (CDGPS) and the on-board Attitude Determination and Control System (ADCS). The authors also describe in detail the capabilities, limitations, and the design of the permanent magnet docking system. One important claim is that this docking system reduces the usage of propellants used for position control in any coarse docking system.

2.4 Docking Mechanism Analysis Papers

Apart from cubesat mission proposals, research papers on the design and analysis of docking mechanisms also help in raising the TRL of small satellite docking systems. Some of these papers have been discussed along with research papers dealing with the modeling of electromagnetic levitation systems.

2.4.1 UDP on SPHERES

The Universal Docking Port [11], designed for the SPHERES facility on-board the ISS is a semi-androgynous docking port designed to provide data and power transfer. The authors describe in detail the complete docking system design and its testing on the SPHERES facility on the ISS. The UDP uses a camera sensor to perform docking in space and has been tested on the SPHERES robots, which are three flying satellites used to test algorithms or other systems. The SPHERES facility with the UDP has also been tested by Miller et al. [15], who proposed an experiment to perform Assembly of a Large Modular Optical Telescope (ALMOST), which was tested while on-board the ISS.

2.4.2 Other Probe and Cone Docking Mechanisms

McCormick et al. [16] propose a robotic manipulator with probe and cone end effectors to demonstrate docking of small satellite clusters. Ye et al. [17] propose an attitude control based probe and cone docking system and discuss the modeling of forces. Zhang et al. [18] also discusses the force modeling of a probe and cone docking system.

2.4.3 ARX Model for Electromagnetic Levitation

Qin et al. [19] propose modeling an electromagnetic levitation system as a Gaussian Radial Basis Function (RBF) Autoregressive (ARX) model. The authors discuss a neural networks based model for the electromagnetic levitation system with a PID controller to control the identified system.

2.4.4 Feedback Linearization of Electromagnetic Levitation Systems

Gandhi et al. [20] and Romero et al. [21] discuss a comparison of feedback linearization of electromagnetic levitation systems and design of various controllers to maintain the ball levitation system in a suspended state.

2.4.5 Mission Comparison

The AAReST mission uses electromagnetic docking system, but with bulky Kinect camera based sensor system, and hasn't been tested in space yet. The CPOD mission uses just a probe and cone docking mechanism, with 4 cameras sensors and an integrated attitude controller strategy, and hasnt been tested in space yet. And the ARCADE-R2 mission used just a probe and cone docking mechanism, with IR LEDs and IR LDR sensors and an integrated attitude controller strategy, but only been tested in the upper atmosphere, but not in space.

Chapter 3

IMPLEMENTATION

This chapter discusses the electromagnetic docking mechanism modeling, control, and simulation. Table 3.1 lists all the objectives and requirements of this thesis work.

Table 3.1: Requirements

	Orbit propagator
1.0	The orbit propagator shall include J2 orbital dynamics of satellites
2.0	The orbit propagator shall be capable of propagating multiple satellites
	Docking system modeling
1.0	The dynamics of an electromagnetic docking system shall be modeled.
	Docking system controller
1.0	Various controller designs for the docking system shall be compared.
2.0	The final docking controller shall be capable of fine docking two small satellites from a given relative distance
3.0	The final docking controller shall have little to no overshoot in the closed loop step response
	Docking system simulation
1.0	The simulation shall demonstrate orbit propagation of two small satellites
2.0	The simulation shall demonstrate docking of two small satellites in orbit

3.1 System Simulation Design

The simulation consists of two parts. The orbit propagator and the docking mechanism. The orbit propagator consists of two satellites going around the Earth in a LEO orbit. The attitude controller is responsible for keeping both the satellites in orbit. It is assumed that the attitude controller has been designed and can get the satellites close enough to dock so that the docking controller can take over and perform fine docking of the satellites. Matlab is chosen to simulate the docking of the two satellites and model the docking mechanism and design a controller for docking. The 3d and 2d animations are generated using Matlab's OpenGL interface, VRML, and the Mapping Toolbox.

3.2 Orbit Propagator

The orbit propagator is responsible for simulating the mechanics of orbit propagation of a general satellite around the Earth in an elliptical orbit. Orbital mechanics is the basis of orbit propagation of any satellite around the Earth. It is divided mainly into orbital kinematics and orbital dynamics [22]. Orbital kinematics deals with the time derivative of a parametrization of the rotation matrix as a function of the angular velocity of the satellite. This implies that the kinematics deals with torques and forces which act on satellites. Orbital mechanics, however, deals with the differential equation for the angular velocity of a satellite, which is derived from Euler's moment equation. Euler's moment equation (Equation 3.1) or rigid body dynamics is a part of classical mechanics which defines the relationship between the angular velocity, ω, torques, M and moment of inertia of a rigid body, I.

$$I\dot{\omega} + \omega \times (I\omega) = M \tag{3.1}$$

For our orbit propagator, it is sufficient to consider orbital dynamics. The basis

of this are the conservation of Energy (Equation 3.2), the conservation of angular momentum (Equation 3.3), and Newton's universal law of gravitation (Equation 3.5).

Conservation of energy states that energy can neither be created nor destroyed, but can be converted from one form to another. Hence, the total energy of a system is constant. In our system, kinetic energy is equal to the gravitational potential energy, which is shown in Equation 3.2.

$$E = \frac{1}{2}mv^2 - \frac{GmM_E}{r} \tag{3.2}$$

Conservation of angular momentum states that the angular momentum of a spinning body is always constant, where L is the total angular momentum, and F_c is the centripetal force, and F_g is the gravitational force.

$$L = mrv \tag{3.3}$$

$$F_c = \frac{mv_c^2}{r} \tag{3.4}$$

$$F_G = \frac{GmM_E}{r^2} \tag{3.5}$$

For a satellite orbiting the Earth, the Gravitational force is equal to the centripetal force. Hence, the centripetal orbital velocity, v_c can be computed as follows.

$$F_c = F_G \tag{3.6}$$

$$\frac{mv_c^2}{r} = \frac{GmM_E}{r^2} \tag{3.7}$$

$$v_c^2 = \frac{GM_E}{r} \tag{3.8}$$

Applying Newton's second law of motion and Newton's law of universal gravity, the differential equation governing the satellite then becomes,

$$m\dot{\vec{v}} = -\vec{F}_G + \vec{F}_{drag} \tag{3.9}$$

The orbit of a satellite is completely defined by these Keplerian orbital elements [23],

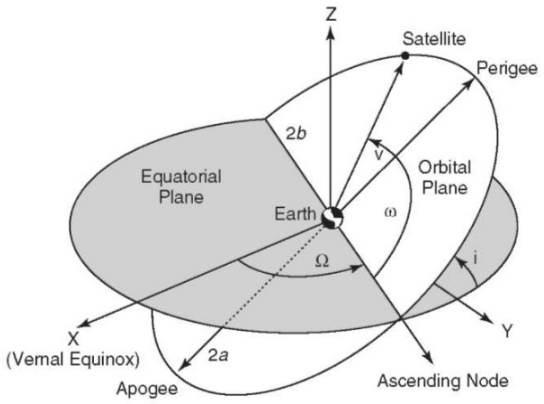

Figure 3.1: Orbital Parameters [1]

Semi-major axis a is one half of the major axis and represents the mean distance from the primary.

Eccentricity e is the ratio of the foci to the length of the major axis.

Inclination i is the angular distance between a satellite's orbital plane and the equation of its primary.

Argument of Perigee ω is the angular distance between the ascending node, the points where an orbital plane crosses from south to north, the equatorial plane, and the perigee, the furthest point from the Earth in the orbit.

Time of Perigee Passage T is the time at which the satellite moves through the perigee.

Right Ascension of Ascending Node (RAAN) Ω is the longitude measured in degrees counter-clockwise to the ascending node from zero longitude being in the direction of the vernal equinox, the place where the sun crosses the Earth's equator, making night and day of approximately equal length all over the Earth.

Time period P is the time required for a satellite to complete one orbit around the Earth.

Mean anomaly M is the angular distance between the perigee and the imagined position of the satellite since the elapsed time, for a circular orbit of the same time period.

Eccentric anomaly E is the angular distance between the perigee and the actual position of the satellite in orbit, measured from the center of the elliptical orbit. Eccentric anomaly must be computed numerically as a function of the mean anomaly and the eccentricity.

$$M = E - e\, sin\, E \tag{3.10}$$

True anomaly f is the angular distance between the perigee and the actual position of the satellite in the direction of motion, measured from the Earth. It is computed as a function of the mean anomaly and the Eccentricity.

$$tan\, \frac{f}{2} = \sqrt{\frac{1+e}{(1-e)\, tan\, \frac{E}{2}}} \tag{3.11}$$

Mean motion M is the angular speed required for a body to complete one orbit, assuming constant speed in a circular orbit of the same time period.

The Keplerian orbital elements computed have to be converted into an Earth Centered Inertial (ECI) Cartesian coordinate form.

$$vec1 = \begin{bmatrix} cos\,\Omega\,cos\,\omega\ - sin\,\Omega\,sin\,\omega\,cos\,i \\ sin\,\Omega\,cos\,\omega\ + cos\,\Omega\,sin\,\omega\,cos\,i \\ sin\,\omega\,sin\,i \end{bmatrix} \tag{3.12}$$

$$vec2 = \begin{bmatrix} -\,cos\,\Omega\,sin\,\omega\ -\ sin\,\Omega\,cos\,\omega\,cos\,i \\ sin\,\Omega\,sin\,\omega\ +\ cos\,\Omega\,cos\,\omega\,cos\,i \\ cos\,\omega\,sin\,i \end{bmatrix} \tag{3.13}$$

$$r = \left(\frac{a\,(1-e^2)}{1+e\,cos\,f}\right) \times \Big(cos\,f\ vec1 + sin\,f\ vec2\Big) \tag{3.14}$$

$$v = \left(\sqrt{\frac{GM}{a\,(1-e^2)}}\right) \times \Big(-\,sin\,f\ vec1 + (e + cos\,f)\ vec2\Big) \tag{3.15}$$

Using these equations, Equation 3.14 is computed for every time instant, as the true anomaly changes over time. Effects of other forces like drag are then computed as in Equation 3.16.

$$r = r + \dot{r}\,(t - t_p) \tag{3.16}$$

$$v = v + \dot{v}\,(t - t_p) \tag{3.17}$$

$\dot{r}$ and $\dot{v}$ are computed for drag force as shown in Equation 3.18. The drag force depends upon ρ, the atmospheric density, C_D, the drag coefficient,A, the area of the satellite in the direction of motion, and m, the mass of the satellite.

$$\frac{\vec{F}_{drag}}{m} = \frac{1}{2}\,\rho\left(\frac{C_D A}{m}\right) v\,\vec{v} \tag{3.18}$$

$$\dot{v} = \frac{\vec{F}_{drag}}{m} \tag{3.19}$$

$$\dot{r} = v \tag{3.20}$$

The orbital parameters used for the simulation are summarized in Table 3.2.

Table 3.2: Orbital Parameters

Parameter	Value
a	6784773.25
e	0.0002623
i	51.34069
ω	120.5358
Ω	233.32704
f_0	201.77697
ρ	1
A	0.03
C_d	2.2

3.3 Attitude Controller

The attitude control system (ACS) of a satellite is responsible for controlling the position and orientation of a satellite and can include de-tumbling the satellite post deployment, pointing the satellite in any given direction, and also performing coarse positioning, ie, bringing the satellites close together in orbit. A standard cubesat ACS will also be accompanied with an attitude determination system (ADS) to sense the attitude of the spacecraft at any given instant of time. Together, they make up the Attitude Determination and Control System (ADCS) [24]. The ADS can consist of various sensors like GPS, star trackers, limb sensors, rate gyros and inertial measurement units. The ACS can consist of actuators like reaction wheels, control moment gyros, magnetic torque rods, and thrusters.

One of the best ways to control the attitude of a spacecraft is to look at torque

control. The disturbances which can affect the attitude of a spacecraft which the ADCS has to deal with are gravity gradient, aerodynamic drag, magnetic torques, solar radiation pressure, mass expulsion, and internal disturbance torques. There are different ways of controlling the attitude of the spacecraft. One such is Passive Attitude Control, where the spacecraft is designed so as to take advantage of the physics of some forces and reduce the effect of others. An example of one such design is Spin Stabilized Spacecrafts, which spin on a particular axis so as to have a stable attitude. Another way of controlling the attitude of a spacecraft is Active Attitude Control, or 3 axis stabilization design. Here, the attitude data from the ADS is used by the ACS to provide the necessary torque commands to the actuators in order to maintain a certain attitude or change it as required. In the case of nanosatellites, and especially in the case of docking, it is best to have 3 axis stabilization.

To perform 3 axis stabilization, we need to know the magnitude of the disturbance torques and the type of sensors and actuators to use and their capabilities. For LEO orbits and nanosatellites, magnetic torques (caused by the Earth), gravity gradient are more significant than atmospheric drag and solar radiation pressure. While magnetic torques and gravity gradient can be of the order of 10^{-5} or 10^{-6}, atmospheric drag and solar radiation pressure can be of the order 10^{-7}. In the case of docking systems, it is essential that the position of the spacecraft is controllable. Thrusters, being one of the most efficient actuators capable of position manipulation in orbit, will have to be used. Thrusters require propellants, which invariably increase the mass and volume of the satellite. Other alternatives can hence be considered but is beyond the scope of this thesis. The ADCS is also responsible for providing coarse positioning. To provide positional control, the satellite has to be equipped with a propulsion system. Thrusters will therefore be used as the actuator to control the position of the satellite in space, to perform orbital maneuvers, shown in Figure 3.2. Orbital maneuvers in

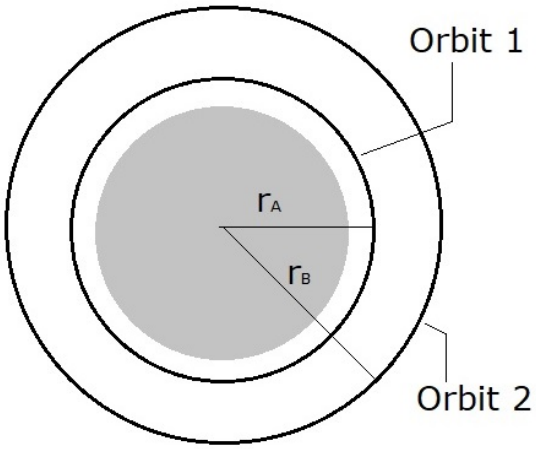

Figure 3.2: Orbital Maneuvering Example

our case includes increasing and decreasing of the eccentricity of the orbit at various points such that the satellites come close to each other in an orbit which can be explained using an example as follows. Consider an scenario where Satellite A and B have a time period P_A and are at an initial distance of $x_1 m$ from each other in the same orbit (measured using the range sensor from the docking system). We know that we want to perform coarse positioning such that the distance between the two satellites is to be reduced to $x_2 m$. To do this, Satellite A will fire the thrusters controlled by the ADCS to increase the eccentricity and hence the period of the satellite to $P_B > P_A$. Satellite A will stay in this period for a pre-calculated time, t_{extra}, so that it accumulates more distance than Satellite B. After time t_{extra}, Satellite A will fire the thrusters, this time to decrease the eccentricity of the orbit, such that it regains the time period P_A, and reducing the distance between the satellites to x_2.

Reducing the distance between the two satellites solves one part of the coarse positioning problem. The next part is to align the satellites so that the docking controller can take over from the ADCS. This can be performed by knowing an approximate position of the satellites. Satellite A, knowing the approximate position of Satellite

B, can use a smart camera or a range sensor which will scan the surroundings and detect the satellite. This will accurately calculate the position of Satellite B, which can then be aligned with the help of the 3-axis stabilization of the ADCS to point in the required direction.

To simulate the second part of coarse positioning, an experiment could be set up, using two robotic arms simulating the ADCS subsystem of the satellites. The robotic arm which is simulating the ADCS of Satellite A will have a camera mounted on it. This can then be used to test the second part of the coarse positioning, while also simulating the docking system. This was demonstrated in a previous work on a smart camera system for tracking meteors [25]. The smart camera system consisted of a camera mounted on a robotic arm, controlled by a Raspberry Pi and a display attached to a computer, which displayed a simulation of random meteor entry events, which is tracked by the robotic arm-camera system. The main components of the system were the meteor tracking system and the meteor simulation system. The meteor tracking system further consisted of the Raspberry Pi, the robotic arm, and the camera, while the meteor simulation system consisted of the meteor simulation control and the meteor simulation itself. The demonstration simulated random meteor entry events. A physics model based simulation of the meteor entry events was displayed on a monitor. The camera mounted on the robotic arm perceived this and image thresholding was performed to detect these meteor events and isolate them from the noise, like lights from the Earth and stars. After this, the trajectory of the meteor was predicted using a predictive model, based on curve fitting based on the trajectory history. Once trajectory prediction was performed, the smart camera system tracked the meteor entry events using the robotic arm. The smart camera system therefore simulated a scaled down, bare minimum version of the tracking system integrated with the ADCS. This smart camera system can be extended to the proposed experimental

setup, by replacing the meteor tracking system with a simulated satellite tracking system and extend the ADCS simulation to the two robotic arms.

For the purpose this thesis, we can assume that the attitude controller has been designed to stabilize the spacecraft and perform coarse positioning.

3.4 Docking System Model

The docking system consists of two parts. It is modeled after the probe and cone docking mechanism. The probe is installed on satellite B, which will dock with the cone installed on satellite A, which is deployed first.

The probe consists of an electromagnetic solenoid wrapped around a core, whose docking end is flat. The docking end of the probe is flat to facilitate a clean docking of the cone. The cone has a latching magnet with sufficient surface area to increase the contact point force while docking so that the need for multiple docking ports is eliminated. The cone is made of a magnetic material so that the probe feels an outward 'pull' and 'push' when it comes close to the cone.

The electromagnetic docking system is modeled as a magnetic levitation system, considering only one axis to control, leaving the alignment to the attitude controller. The electromagnetic docking system is modeled using first principles as in Equation 3.21 and Equation 3.27. Here, $i(t)$ is current flowing through the circuit, $u(t)$ is the voltage input, R is the resistance of the electromagnetic circuit, N is the number of turns of the electromagnetic coil, $L_1 = \frac{N^2}{Rl}$ is the self-inductance of the electromagnetic coil, $L(y)$ is the mutual inductance of the probe and cone system, which is a function of y, the distance between them, Rl is the reluctance of the electromagnetic circuit, μ_0 is the permeability of free space, A is the effective area of the solenoid core of the probe influencing the cone, m is the mass of the satellite, and F_{ext} is the external force, either gravitational or other forces.

$$\frac{di}{dt} = \frac{1}{L_1}\,u(t) \; - \frac{R}{L_1}\,i \tag{3.21}$$

$$\frac{d^2y}{dt^2} = -\frac{F(y,i)}{m} \; + \; \frac{F_{ext}}{m} \tag{3.22}$$

$$F(y,i) = -\frac{d}{dt}\left[\frac{1}{2}\,L(y)\,i^2(t)\right] \tag{3.23}$$

$$L(y) = \frac{\mu_0 N^2 A}{2y(t)} \tag{3.24}$$

$$F(y,i) = \frac{\mu_0 N^2 A}{l}\left[\frac{i(t)}{y(t)}\right]^2 \tag{3.25}$$

$$F(y,i) = k\left[\frac{i(t)}{y(t)}\right]^2 \tag{3.26}$$

$$\frac{d^2y}{dt^2} = -\frac{k}{m}\left[\frac{i(t)}{y(t)}\right]^2 \; + \; \frac{F_{ext}}{m} \tag{3.27}$$

The docking mechanism is converted into a state space model as in Equation 3.28 with states $x_1 = y$, $x_2 = \dot{y}$, $x_3 = i(t)$, and y as the output of the system.

$$\left.\begin{aligned} \dot{x}_1 &= x_2 \\ \dot{x}_2 &= -\frac{k}{m}\left[\frac{x_3}{x_1}\right]^2 \; + \; \frac{F_{ext}}{m} \\ \dot{x}_3 &= -\frac{R}{L_1}\,x_3 \; + \frac{1}{L_1}\,u \\ y &= x_1 \end{aligned}\right\} \tag{3.28}$$

This system is of the form,

$$\dot{x} = f(x) + g(x)u \tag{3.29}$$

$$y = h(x) \tag{3.30}$$

The values of the parameters considered are summarized in Table 3.3.

Table 3.3: Docking System Parameters

Parameter	Value
m	3
R	4.2
N	4500
μ_0	1.26×10^{-6}
A	0.00785
l	0.1
L_1	0.02
F_{ext}	2.058
d	1

3.5 Docking Controller Design

Various controller design techniques are discussed in this section. In order to control the dynamics of the docking mechanism using linear controls, we need to make sure the system is linear. The docking mechanism system is considered as our plant which has nonlinear dynamics. We would therefore need to linearize the plant first. This section discusses two linearization techniques and multiple linear controller designs which are explained in detail.

3.5.1 Taylor Series Linearization

The first technique is to linearize the plant around the equilibrium point, using Taylor series expansion method.

The system is defined to be of the form,

$$\dot{x} = f(x) + g(x)u = F(x, u) \tag{3.31}$$

$$y = h(x) \tag{3.32}$$

Let us consider the equilibrium conditions at states x_e and derive a Taylor series expansion of the system at the equilibrium conditions to linearize it. At the equilibrium point, there is no change in the states of a system.

$$\text{i.e., } \dot{x} = 0 \text{ or, } F(x_e, u_e) = 0 \tag{3.33}$$

$$\dot{x}_1 = x_2 = 0 \tag{3.34}$$

$$\dot{x}_2 = -\frac{k}{m}\left[\frac{x_3}{x_1}\right]^2 + \frac{F_{ext}}{m} = 0 \tag{3.35}$$

$$\dot{x}_3 = -\frac{R}{L_1}\, x_3 + \frac{1}{L_1}\, u = 0 \tag{3.36}$$

$$x_3 = \frac{u}{R} \tag{3.37}$$

$$x_1 = \frac{u}{R}\sqrt{\frac{k}{F_{ext}}} \tag{3.38}$$

$$\text{Let } x_1 = d \tag{3.39}$$

$$u = Rd\sqrt{\frac{F_{ext}}{k}} \tag{3.40}$$

$$x_3 = d\sqrt{\frac{F_{ext}}{k}} \tag{3.41}$$

$$\left.\begin{aligned} x_e = \begin{bmatrix} x_1 \\ x_2 \\ x_3 \end{bmatrix} = \begin{bmatrix} d \\ 0 \\ d\sqrt{\frac{F_{ext}}{k}} \end{bmatrix} \\ \text{and, } u_e = Rd\sqrt{\frac{F_{ext}}{k}} \end{aligned}\right\} \tag{3.42}$$

Now that we have found the equilibrium points,

$$\Delta\dot{x} = \cancelto{0}{F(x_e, u_e)} + \Delta x \left.\frac{\partial F(x,u)}{\partial x}\right|_{\substack{x=x_e,\\ u=u_e}} + \Delta u \left.\frac{\partial F(x,u)}{\partial u}\right|_{\substack{x=x_o,\\ u=u_o}} \tag{3.43}$$

$$\Delta y = \Delta x \left.\frac{\partial h(x)}{\partial x}\right|_{\substack{x=x_e,\\ u=u_e}} \tag{3.44}$$

$$\tag{3.45}$$

The Δx in the then replaced by x and will be of the form,

$$\dot{x} = Ax + Bu \tag{3.46}$$

$$y = Cx \tag{3.47}$$

3.5.2 Bandwidth and Robustness Controller Design

Now that we have linearized the system, we can design various controllers to control the separation distance, y of the system. One such controller design is Bandwidth and Robustness Controller design [26]. In this technique, we first decide the required bandwidth and phase margin of the open loop system, which includes the plant and the controller, where the electromagnetic docking system is considered as the plant. Figure 3.3 shows the block diagram of a standard control system. The controller can be replaced by the designed BW and robustness controller or PID or LQG. In the figure, the pre-filter, W, is used to attenuate the overshoot in the system caused by the zeros in the controller, and is represented as $W(s) = \frac{\text{zeros in the controller}}{\text{factor to make the gain of W unity}}$.

Phase margin, PM of a system is the phase of the system at the gain crossover frequency. The gain crossover frequency, ω_g , is that frequency at which the magnitude of the system is unity. The bandwidth, or the closed loop bandwidth of a system is proportional to the inverse of the rise time of the step response of the closed loop system. Sometimes, it can be considered as 35 % of the inverse of the rise time. The

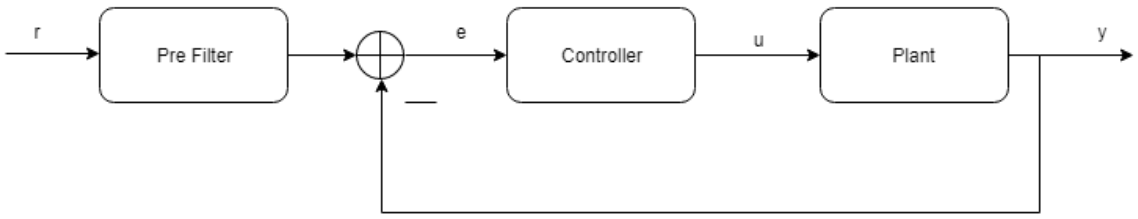

Figure 3.3: Standard Form of a Feedback Control System with Plant as P(s)

rise time of a system is the time required for the response to rise from 10 % to 90% of its final value or the steady state value.

To design any controller, we have to first check for reference command following. This is governed by the Internal Model Principle, which states that, for the output to follow a signal, its model has to be in the forward path, and that for the output to reject a signal, its model has to be present outside the forward path, somewhere in the feedback loop. We want the system to follow step commands, hence, we should include an integrator in the forward path of the closed loop feedback system. If the plant has a transfer function $P_0(s)$, we have to append an integrator, $\frac{1}{s}$ before the system and the new plant will be $P(s) = \frac{P_0(s)}{s}$.

In the bandwidth and robustness controller design, we assume the structure of a controller as in Equation 3.48. Then, the number of zeros is calculated for the system, considering that only 60° is contributed by one zero. Then, using the phase $\angle P(j\omega_g)$ of the plant P at ω_g, we can compute the zero, z. For this, we assume that the pseudo-pole of the controller, τ is 4% of the inverse of ω_g, by common rule of thumb (As τ is half the sampling time and the sampling time should be considered as 8% of the inverse of the bandwidth). After this, the gain, g is calculated using the

fact that $|L(j\omega_g)| = 1$, where L is the open loop transfer function of the system.

$$K = \frac{g(s+z)^n}{s(\tau s+1)} \tag{3.48}$$

$$L = PK \tag{3.49}$$

$$\text{PM} = 180^\circ + \angle L(j\omega_g) \tag{3.50}$$

$$\angle Zero_{total} = \text{PM} - 90 + \tan^{-1}(\tau\omega_g) \tag{3.51}$$

$$n = max(\frac{\angle Zero_{total}}{60}) \tag{3.52}$$

$$z = \frac{\omega_g}{tan(\frac{\angle Zero_{total}}{n})} \tag{3.53}$$

$$|L(j\omega_g)| = |K(j\omega_g)||P(j\omega_g)| \tag{3.54}$$

$$g = \frac{\omega_g}{|P(j\omega_g)|}\sqrt{\frac{\omega_g^2\tau^2+1}{(\omega_g^2+z^2)^n}} \tag{3.55}$$

3.5.3 PID Controller Design

The next type of controller design is the standard PID controller as in Equation 3.56. One common way of designing this is to use Ziegler-Nichols (ZN) tuning. We use the second method out of the two ZN tuning methods. Both the methods use the step response of the system. The first method uses the open loop step response to compute the slope R and delay L of the response, in order to compute the K_p, K_i, K_d values. The second method however uses the closed loop step response to compute the ultimate gain K_u and period of oscillations P_u in order to compute the K_p, K_i, K_d values. Here, the ultimate gain is that gain at which the closed loop step response of the system becomes oscillatory and the period of oscillations is as the name suggests. The relationship between the gains and the parameters is summarized in Table 3.4 and Table 3.5.

$$K = K_p + \frac{K_i}{s} + \frac{K_d s}{\tau s+1} \tag{3.56}$$

Table 3.4: Ziegler-Nichols Tuning Method 1

Controller	K_p	K_i	K_d
P	$\frac{1}{RL}$	-	-
PI	$\frac{0.9}{RL}$	$\frac{0.27}{RL^2}$	-
PID	$\frac{1.2}{RL}$	$\frac{0.6}{RL^2}$	$\frac{0.5}{R}$

Table 3.5: Ziegler-Nichols Tuning Method 2

Controller	K_p	K_i	K_d
P	$0.5K_u$	-	-
PI	$0.45K_u$	$\frac{0.54K_u}{P_u}$	-
PID	$0.6K_u$	$\frac{1.2K_u}{P_u}$	$0.075K_uP_u$
PID No overshoot	$0.2K_u$	$\frac{0.1K_u}{P_u}$	$0.2K_uP_u$

3.5.4 Linear Quadratic Gaussian Controller Design

The next type of controller design is the Linear Quadratic Gaussian(LQG) controller. This is a combination of the Linear Quadratic Regulator (LQR) and the Kalman Filter (KF). The LQR controller is designed by solving the Control Algebraic Riccati Equation (CARE). The LQR guarantees that the closed loop system is asymptotic stable. It also guarantees that the feedback law is the optimal control minimizing the cost function,

$$J(u) = \frac{1}{2}\int_0^\infty \{x^T Q x + u^T R u\}\, dt \tag{3.57}$$

where x is the state vector, u is the input vector, $Q = C^T C$, where C is the output matrix of the plant, $R = \rho I$ regulates how much control is to be used to control the system, either cheap control or expensive control, regulated by ρ. The LQR also

guarantees that the downward gain margin of the system will be less than half, the upward gain margin of the system will be infinity, and that the phase margin of the system will be greater than or equal to 60°.

The CARE equation is shown in Equation 3.58, where we solve for K, which is a symmetric matrix, and A & B are the state and input matrices of the plant respectively. Using K from the solution to CARE, we can compute G, which is the control gain matrix.

$$0 = KA + A^T K + M^T M - KBG \tag{3.58}$$

$$M = Q^{\frac{1}{2}} \tag{3.59}$$

$$G = R^{-1} B^T K \tag{3.60}$$

The Kalman Filter is realised by solving the Filter Algebraic Riccati Equation (FARE) Equation 3.61. FARE is analogous to CARE, and hence can be realised as a modified version of CARE Table 3.6. H is the state estimation matrix.

$$0 = \Sigma A^T + A\Sigma + LL^T - HC\Sigma \tag{3.61}$$

$$H = \Sigma C^T \Theta^{-1} \tag{3.62}$$

Table 3.6: CARE and FARE Analogies

CARE	FARE
A	A^T
B	C^T
M	L^T
R	Θ^T
ρ	μ
K	Σ^T
G	H^T

Using the computed values for G and H, we can define our controller, K of the form Equation 3.63. A block diagram representing this transformation for a model based compensator is shown in Figure 3.4.

$$K = C_k(sI - A_k)^{-1}B_k \tag{3.63}$$

$$\dot{x} = A_k x + B_k e \tag{3.64}$$

$$u = C_k x \tag{3.65}$$

where,

$$A_k = A - BG - H(C - DG) \tag{3.66}$$

$$B_k = -H \tag{3.67}$$

$$C_k = -G \tag{3.68}$$

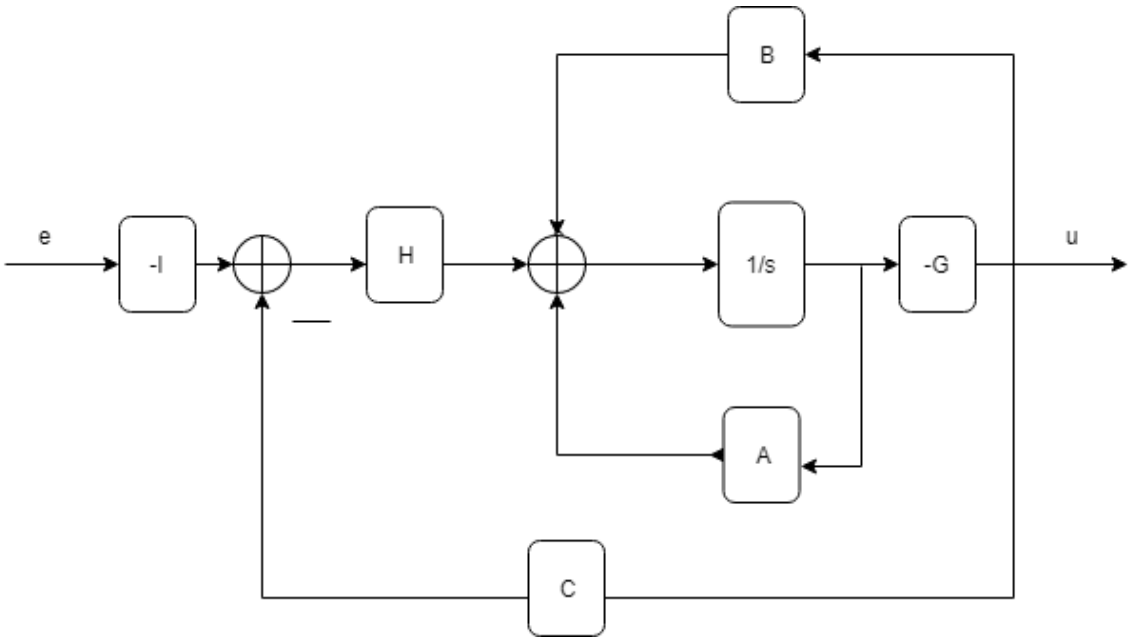

Figure 3.4: Model Based Compensator for Combining LQR and Kalman Filter

3.5.5 Feedback Linearization

We have looked at Taylor Series Linearization, which assumes that the operating point of the system is near the equilibrium point. This does not work well with highly nonlinear systems, like the docking mechanism. Let us recap the type of plant we

have.

$$\dot{x} = f(x) + g(x)u \tag{3.69}$$

$$y = h(x) \tag{3.70}$$

where,

$$f(x) = \begin{bmatrix} x_2 \\ -\frac{k}{m}\left(\frac{x_3}{x_1}\right)^2 + \frac{F_{ext}}{m} \\ -\frac{R}{L_1}x_3 \end{bmatrix} \tag{3.71}$$

$$g(x) = \begin{bmatrix} 0 \\ 0 \\ \frac{1}{L_1} \end{bmatrix} \tag{3.72}$$

$$h(x) = \begin{bmatrix} x_1 \\ 0 \\ 0 \end{bmatrix} \tag{3.73}$$

For such a plant, we can perform feedback linearization [27] to design a control law of the form Equation 3.74, where v is the new transformed input. There are two kinds of feedback linearization, input-output linearization and state-space linearization. The premise of feedback linearization is that the input is nonlinear transformed, which leaves the modified states linear. However, the premise of input-output linearization method is that the plant can be expressed in terms of states which are nonlinear, but linear in the input-output relation. We will discuss input-output linearization alone. Similar theory can then be applied to state-space linearization.

$$u = a(x) + b(x)v \tag{3.74}$$

The first step in feedback linearization is to find the Lie derivatives $L_{()}()$ of $h(x)$

and $g(x)$ with respect to $f(x)$.

$$L_f h(x) = \frac{\partial h(x)}{\partial x} f(x) \tag{3.75}$$

$$L_f h(x) = \begin{bmatrix} \frac{\partial h}{\partial x_1} & \frac{\partial h}{\partial x_2} & \frac{\partial h}{\partial x_3} \end{bmatrix} \begin{bmatrix} f_1(x) \\ f_2(x) \\ f_3(x) \end{bmatrix} \tag{3.76}$$

$$L_f h(x) = \begin{bmatrix} 1 & 0 & 0 \end{bmatrix} \begin{bmatrix} x_2 \\ -\frac{k}{m}\left(\frac{x_3}{x_1}\right)^2 + \frac{F_{ext}}{m} \\ -\frac{R}{L_1} x_3 \end{bmatrix} \tag{3.77}$$

$$L_f h(x) = x_2 \tag{3.78}$$

$$L_f L_f h(x) = L_f^2 h(x) = \frac{\partial L_f h(x)}{\partial x} f(x) \tag{3.79}$$

$$L_f^2 h(x) = \begin{bmatrix} 0 & 1 & 0 \end{bmatrix} \begin{bmatrix} x_2 \\ -\frac{k}{m}\left(\frac{x_3}{x_1}\right)^2 + \frac{F_{ext}}{m} \\ -\frac{R}{L_1} x_3 \end{bmatrix} \tag{3.80}$$

$$L_f^2 h(x) = f_2(x) = -\frac{k}{m}\left(\frac{x_3}{x_1}\right)^2 + \frac{F_{ext}}{m} \tag{3.81}$$

$$L_g L_f h(x) = \frac{\partial L_f h(x)}{\partial x} g(x) \tag{3.82}$$

$$L_g L_f h(x) = \begin{bmatrix} 0 & 1 & 0 \end{bmatrix} \begin{bmatrix} 0 \\ 0 \\ \frac{1}{L_1} \end{bmatrix} \tag{3.83}$$

$$L_g L_f h(x) = 0 \tag{3.84}$$

$$L_f^3 h(x) = \frac{\partial L_f^2 h(x)}{\partial x} f(x) \tag{3.85}$$

$$L_f^3 h(x) = \begin{bmatrix} \frac{2kx_3^2}{mx_1^3} & 0 & -\frac{2kx_3}{mx_1^2} \end{bmatrix} \begin{bmatrix} x_2 \\ -\frac{k}{m}\left(\frac{x_3}{x_1}\right)^2 + \frac{F_{ext}}{m} \\ -\frac{R}{L_1} x_3 \end{bmatrix} \tag{3.86}$$

$$L_f^3 h(x) = \frac{2kx_3^2}{mx_1^2}\left(\frac{x_2}{x_1} + \frac{R}{L_1}\right) \tag{3.87}$$

$$L_g L_f^2 h(x) = \frac{\partial L_f^2 h(x)}{\partial x} g(x) \tag{3.88}$$

$$L_g L_f^2 h(x) = \begin{bmatrix} \frac{2kx_3^2}{mL_1x_1^3} & 0 & -\frac{2kx_3}{mL_1x_1^2} \end{bmatrix} \begin{bmatrix} 0 \\ 0 \\ \frac{1}{L_1} \end{bmatrix} \tag{3.89}$$

$$L_g L_f^2 h(x) = -\frac{2kx_3}{mL_1x_1^2} \tag{3.90}$$

We compute till the third degree of Lie derivative as the relative degree of the system r is 3. The relative degree of a nonlinear system is the smallest integer r for which $L_g L_f^{r-1} h(x) \neq 0$ and $L_g L_f^{r-2} h(x) = 0 \; \forall \; x$ in the neighborhood of the defined operating point x_0.

The system equation can then be represented as,

$$y = h(x) \tag{3.91}$$

$$\dot{y} = L_f h(x) \tag{3.92}$$

$$\ddot{y} = L_f^2 h(x) \tag{3.93}$$

$$\dddot{y} = L_f^3 h(x) + L_g L_f^2 h(x) \tag{3.94}$$

We can then define a nonlinear state transformation as follows.

$$z = T(x) \tag{3.95}$$

$$z = \begin{bmatrix} z_1(x) \\ z_2(x) \\ z_3(x) \end{bmatrix} = \begin{bmatrix} y \\ \dot{y} \\ \ddot{y} \end{bmatrix} \tag{3.96}$$

$$z = \begin{bmatrix} x_1 \\ x_2 \\ -\frac{k}{m}\left(\frac{x_3}{x_1}\right)^2 + \frac{F_{ext}}{m} \end{bmatrix} \tag{3.97}$$

$$\dot{z} = \begin{bmatrix} \dot{z_1} \\ \dot{z_2} \\ \dot{z_3} \end{bmatrix} \tag{3.98}$$

$$\dot{z} = \begin{bmatrix} x_2 \\ -\frac{k}{m}\left(\frac{x_3}{x_1}\right)^2 + \frac{F_{ext}}{m} \\ \frac{2kx_3^2}{mx_1^2}\left(\frac{x_2}{x_1} + \frac{R}{L_1}\right) \end{bmatrix} + \begin{bmatrix} 0 \\ 0 \\ -\frac{2kx_3}{mL_1x_1^2} \end{bmatrix} u \tag{3.99}$$

Here, z is the new state vector. And if $\dot{z_3} = v$, then $v = -Kz$ becomes the new state feedback control law. The input-output feedback transformation then can be represented in terms of the relation between u and v as,

$$u = \frac{1}{L_g L_f^2 h(x)}\big(- L_f^3 h(x) + v\big) \tag{3.100}$$

$$u = \frac{-1}{\frac{2kx_3}{mL_1x_1^2}}\big(- \frac{2kx_3^2}{mx_1^2}\big(\frac{x_2}{x_1} + \frac{R}{L_1}\big) + v\big) \tag{3.101}$$

$$u = x_3\left[\frac{x_2L_1}{x_1} + R\right] - \frac{mL_1x_1^2}{2kx_3}v \tag{3.102}$$

Using the transformation in Equation 3.102 and Equation 3.95, we can design a

linear system of the form,

$$P_{Lin} = C_l(sI - A_l)^{-1}B_l \tag{3.103}$$

$$\dot{z} = A_l z + B_l v \tag{3.104}$$

$$y = C_l z \tag{3.105}$$

where,

$$A_l = \begin{bmatrix} 0 & 1 & 0 \\ 0 & 0 & 1 \\ 0 & 0 & 0 \end{bmatrix} \tag{3.106}$$

$$B_l = \begin{bmatrix} 0 \\ 0 \\ 1 \end{bmatrix} \tag{3.107}$$

$$C_l = \begin{bmatrix} 1 & 0 & 0 \end{bmatrix} \tag{3.108}$$

P_{Lin} from Equation 3.103 can then be controlled either by a full state feedback of the form $v = -Kz$ or an LQG Controller as in Equation 3.63. LQG controller will be a more robust controller than just full state feedback. Hence, LQG is implemented after feedback linearization.

3.6 Simulation Integration

The satellite orbit propagator and the docking system were independently designed, considering appropriate values for various parameters. The attitude control system is integrated with the orbit propagator and is assumed that the simulation starts when the two satellites which need to be docked are de-tumbled and perform attitude corrections, in order for satellite B to get close enough to satellite A for the fine docking system, the docking controller to takeover.

To complete the system, the orbit propagator simulation has to be combined with the output docking system, which takes a feedback of the relative distance between the satellites. The completed simulation includes a real-time 3d and 2d visualization of the satellites orbiting the Earth, and a real-time docking of the two satellites in orbit.

Chapter 4

MISSION CONCEPT

Mission Statement This work proposes a cubesat mission with two 3U cubesats, Satellite A having the probe part of the docking system and Satellite B having the cone part of the docking system. Satellite A is responsible for docking with Satellite B. This mission serves as a demonstration for future in-space assembly and repair missions for cubesats by developing an electromagnetic probe and cone docking system. This docking system will have coarse positioning provided by the ADCS of the small satellite and fine docking provided by the docking controller.

4.1 System Architecture

Figure 4.1 shows how the preliminary version docking system will look like. Figure 4.2 and Figure 4.3 show how the docking system interfaces with the rest of the cubesat. The docking system can be considered as an add-on module pair which will have to be installed on the satellites. The probe docking system will be installed on Satellite A and the cone docking system will be installed on Satellite B.

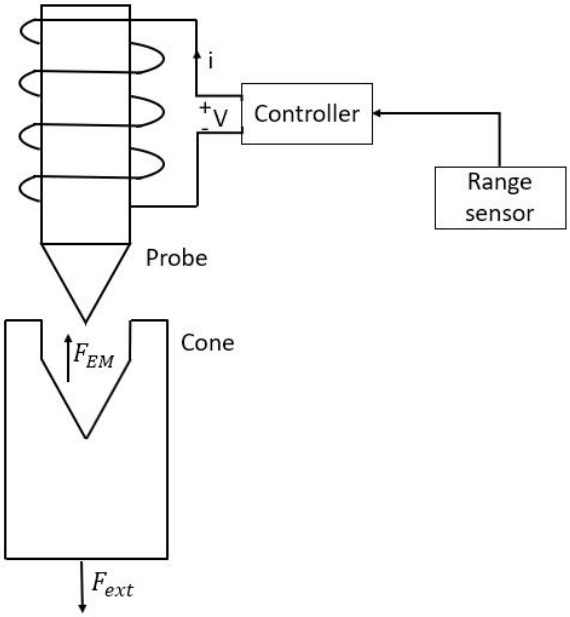

Figure 4.1: Docking System Architecture

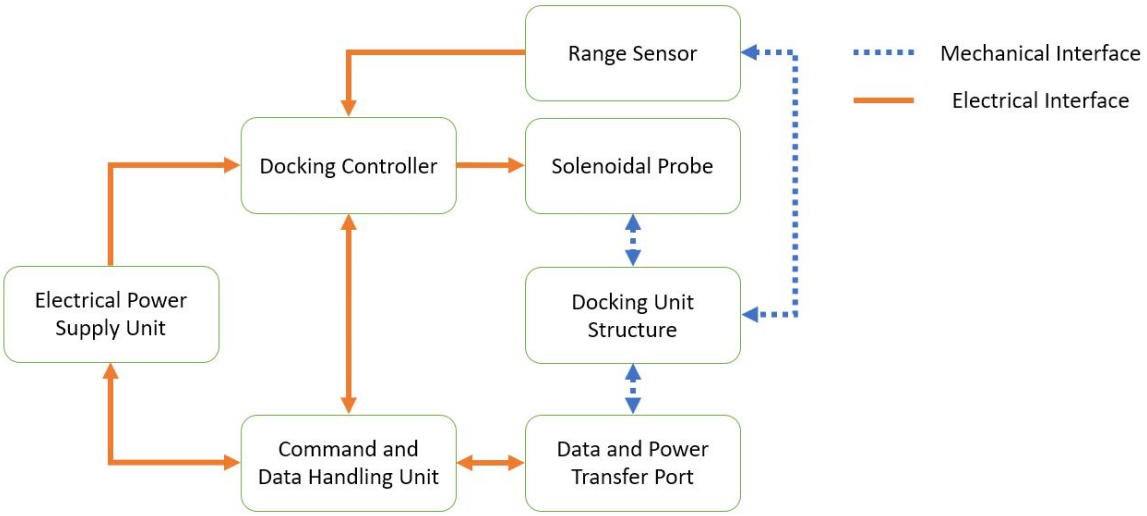

Figure 4.2: Satellite A (Probe) Docking System Interface Diagram

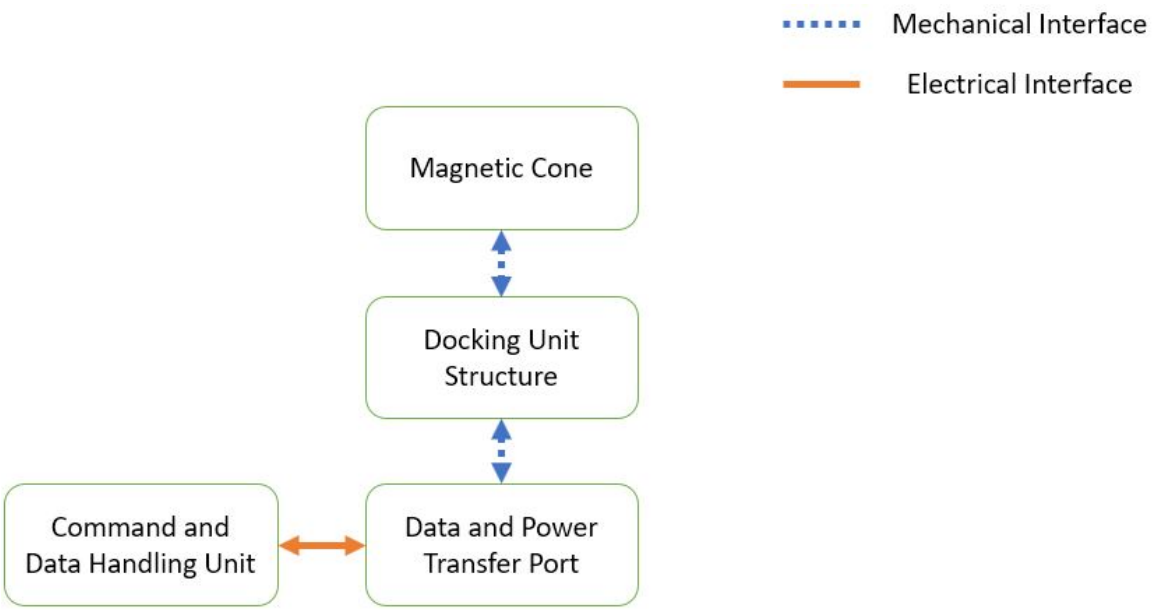

Figure 4.3: Satellite B (Cone) Docking System Interface Diagram

4.2 ConOps

The concept of operations of the mission is shown in Figure 4.4. The mission has 2 main stages, the coarse positioning stage which will be performed by the ADCS and the fine docking stage which will be performed by the docking system.

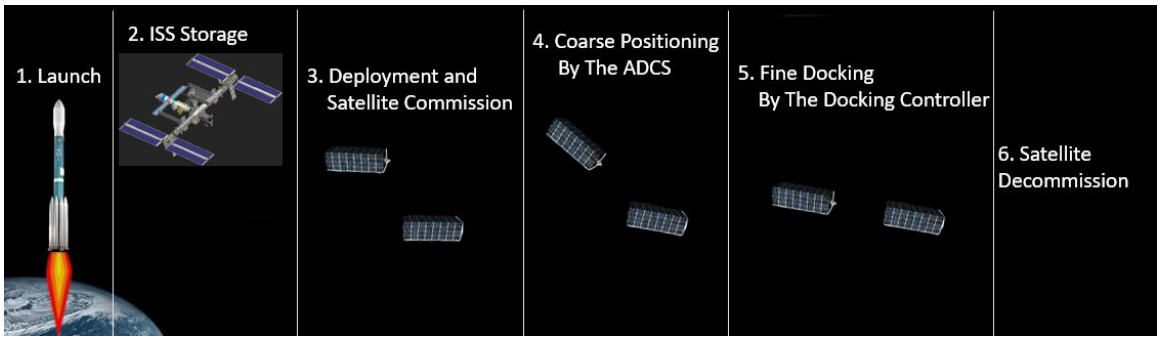

Figure 4.4: Concept of Operations

4.3 Objectives

The primary and secondary mission objectives are enumerated in Table 4.1. Table 4.2 lists the requirements of the subsystems which pertain to this thesis, the ADCS subsystem and the docking system.

Table 4.1: Mission Objectives

	Primary Objectives
1.0	Perform docking of two small satellites in space
2.0	Demonstrate the capability of the docking controller to fine dock two small satellites
	Secondary Objectives
3.0	Demonstrate the capability of the ADCS to coarse position two small satellites
4.0	Demonstrate the capability of data and power transfer between the small satellites

Table 4.2: System Requirements

	ADCS requirements
1.0	Both the small satellites will be capable of attitude determination and control
2.0	Both the small satellites will be capable of detumbling after deployment
3.0	Both the small satellites will be capable of pointing
4.0	Satellite A will be capable of determining the position of Satellite B at any given time
5.0	Satellite A will be capable of position control
6.0	Satellite A will be capable of performing coarse positioning from an initial separation to up to TBD meter relative distance between the two satelites
	Docking system requirements
1.0	Satellite A will be capable of sensing the relative distance between the two small satellites
2.0	Satellite A will be capable of performing fine docking to get from an initial separation to perfectly dock with Satellite B
3.0	There will be little to no force exerted by Satellite A when it docks Satellite B

Chapter 5

RESULTS

5.1 Docking System Plots

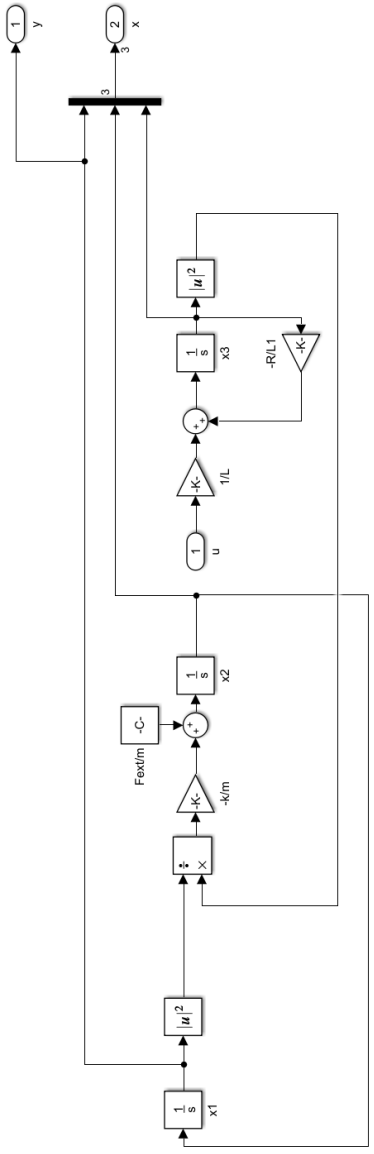

Figure 5.1: Electromagnetic Docking System Nonlinear Model

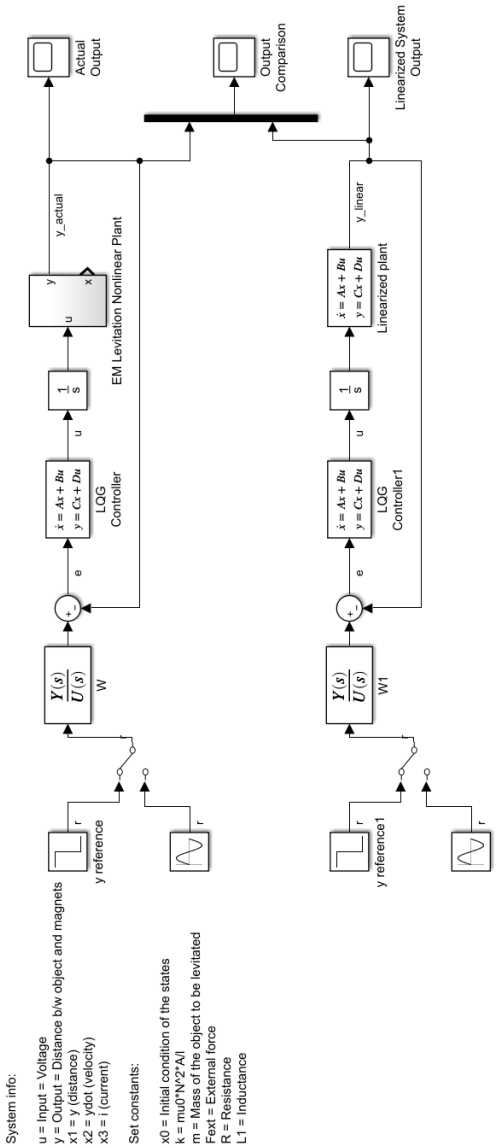

Figure 5.2: Taylor Series Linearized Nonlinear System with LQG Controller

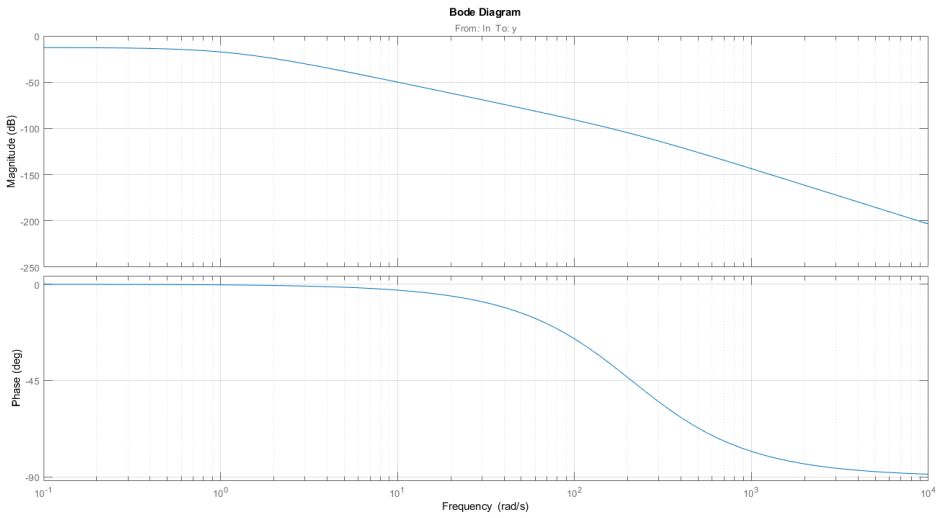

Figure 5.3: Bode Plot of the Taylor Series Linearized Nonlinear System

The simulink block diagram of the nonlinear plant is shown in Figure 5.1 and its Taylor series linearized implementation with a controller in the closed loop is shown in Figure 5.2. An integrator is included in the closed loop system before the plant to facilitate reference command following according to the internal model principle. page 48 shows the frequency response of the Taylor series linearized plant.

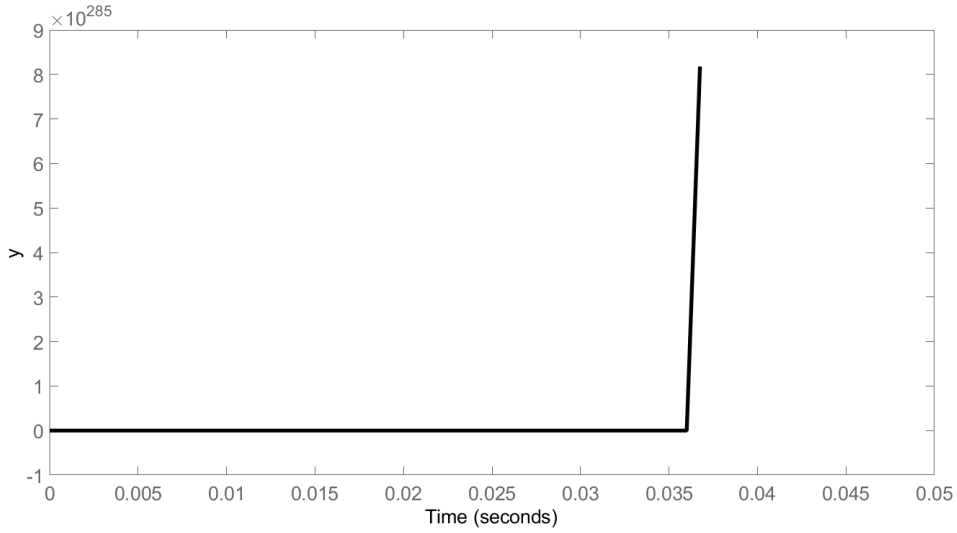

Figure 5.4: Taylor Series Linearized Nonlinear System with Bandwidth and Robustness Controller Design

The step response of the first type of controller design is shown in Figure 5.4. It is seen that even the closed loop linearized system is unstable. A bandwidth of 5.2×10^3 and a phase margin of $60°$ is considered for the design, which can be picked from the bode plot of the plant.

Since BW and Robustness controller design did not work for the system, a PID controller design is looked at. Figure 5.5 shows the step response of the system with a PID controller. It is seen from the response that this too is unstable due to the fragile stability of the closed loop system.

The next controller design considered is the LQG controller design, the step response of which is shown in Figure 5.6. The response indicates that the closed loop system is stable and has good reference command following properties. However, when the same controller is tested with the actual nonlinear system in the loop, the closed loop system becomes unstable, as shown in Figure 5.7.

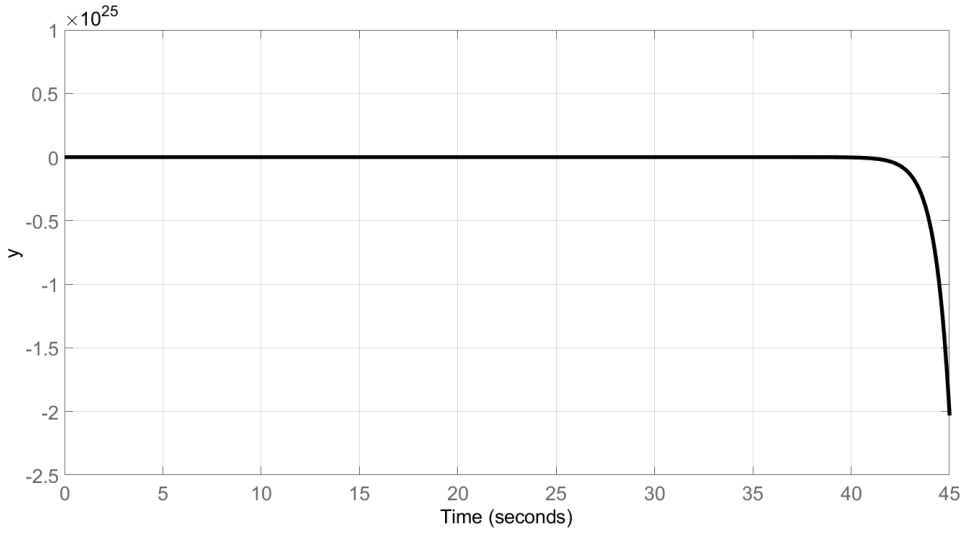

Figure 5.5: Taylor Series Linearized Nonlinear System with PID Controller Design

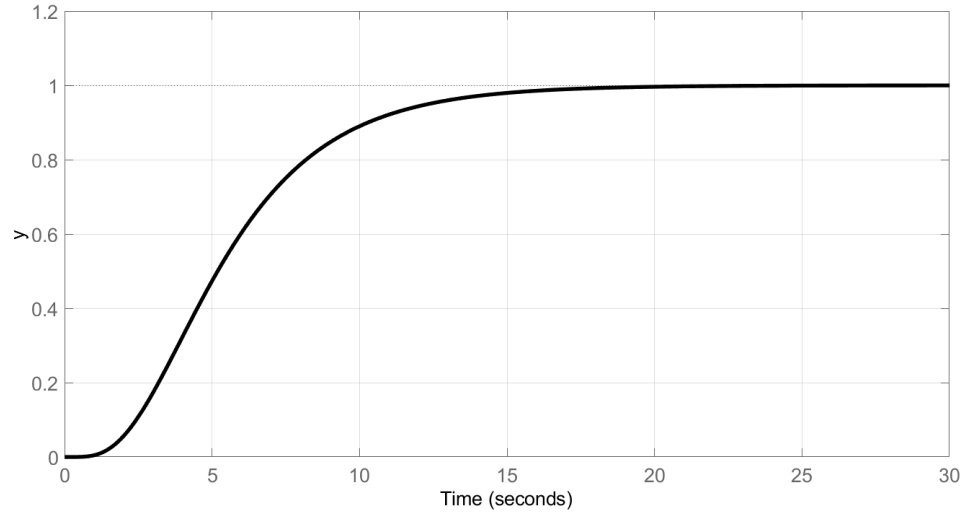

Figure 5.6: Taylor Series Linearized Nonlinear System with LQG Controller Design

Theoretical Output

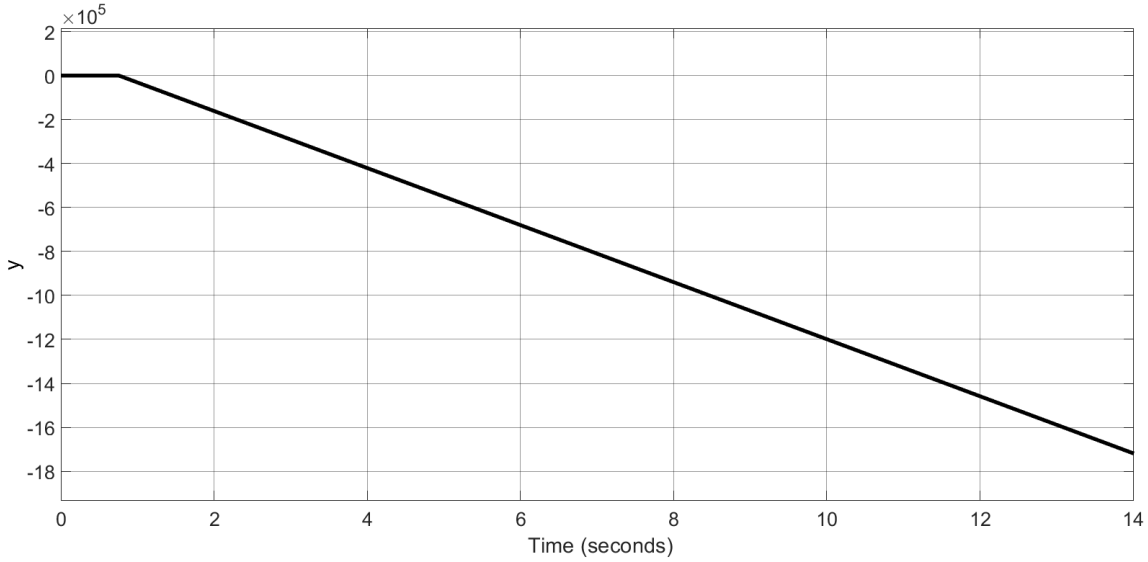

Figure 5.7: Taylor Series Linearized Nonlinear System with LQG Controller Design Actual Output

The step response of the theoretical linearized system with the actual non linear system with the LQG controller is shown in Figure 5.8 and Figure 5.9. While the former shows the magnitude of variation between the theoretical and the actual system, the latter gives a clear comparison of how soon the actual system deviates from the theoretical linearized model.

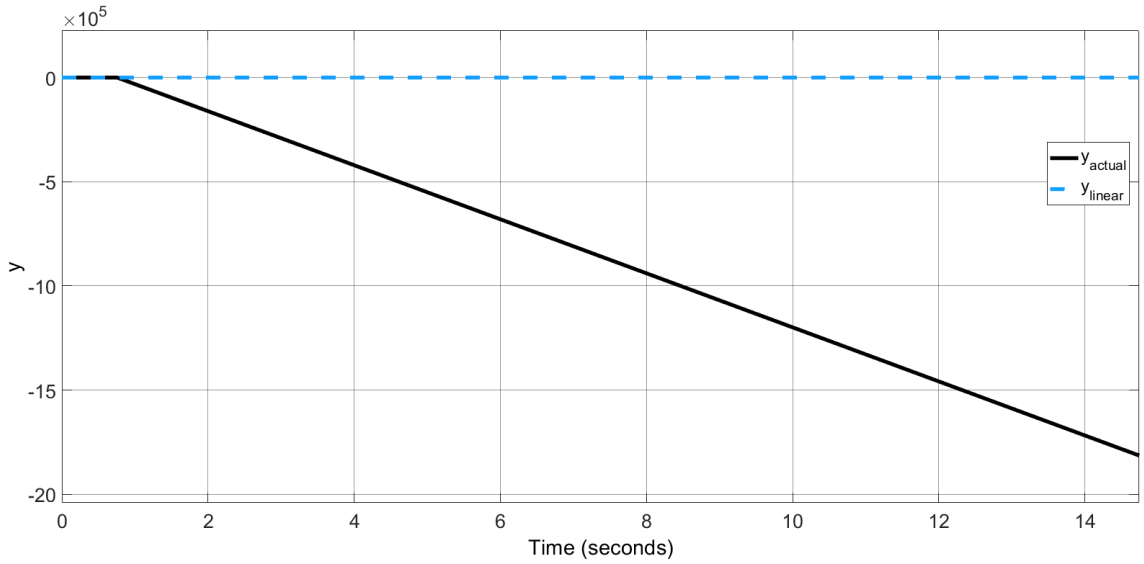

Figure 5.8: Taylor Series Linearized Closed Loop System Output Comparison

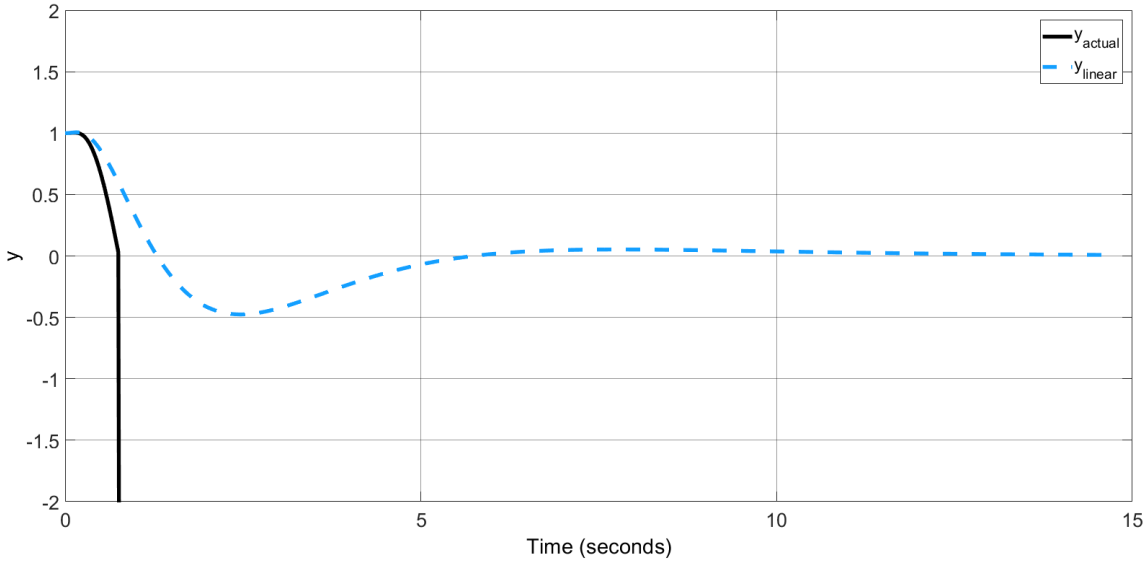

Figure 5.9: Taylor Series Linearized Closed Loop System Output Comparison

The next few figures show Feedback Linearization is implemented for the nonlinear system and how the system performs. Figure 5.10 shows the implementation of the state conversion from x to z. Figure 5.11 shows the input conversion from u to v, so that input-output linearization is performed. It is important to note the voltage saturation block in this figure, set to $\pm 10V$. Figure 5.12 shows the implementation of the complete closed loop system with an LQG controller and a comparison between the theoretical feedback linearized system and the actual nonlinear system with input output linearization.

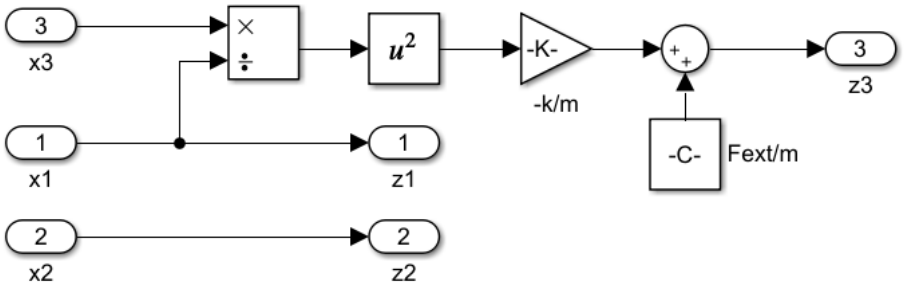

Figure 5.10: Feedback Linearized Nonlinear System State Converter

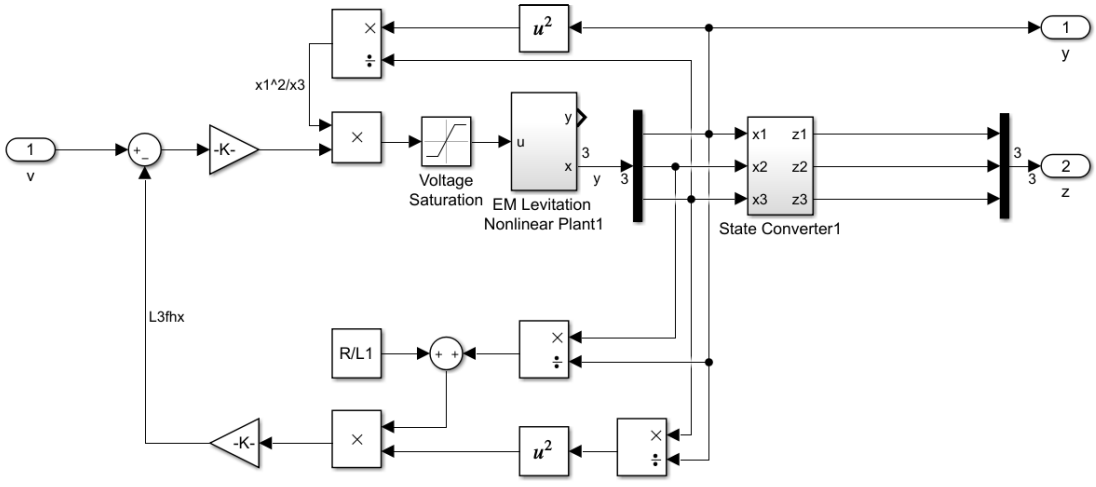

Figure 5.11: Feedback Linearized Nonlinear System

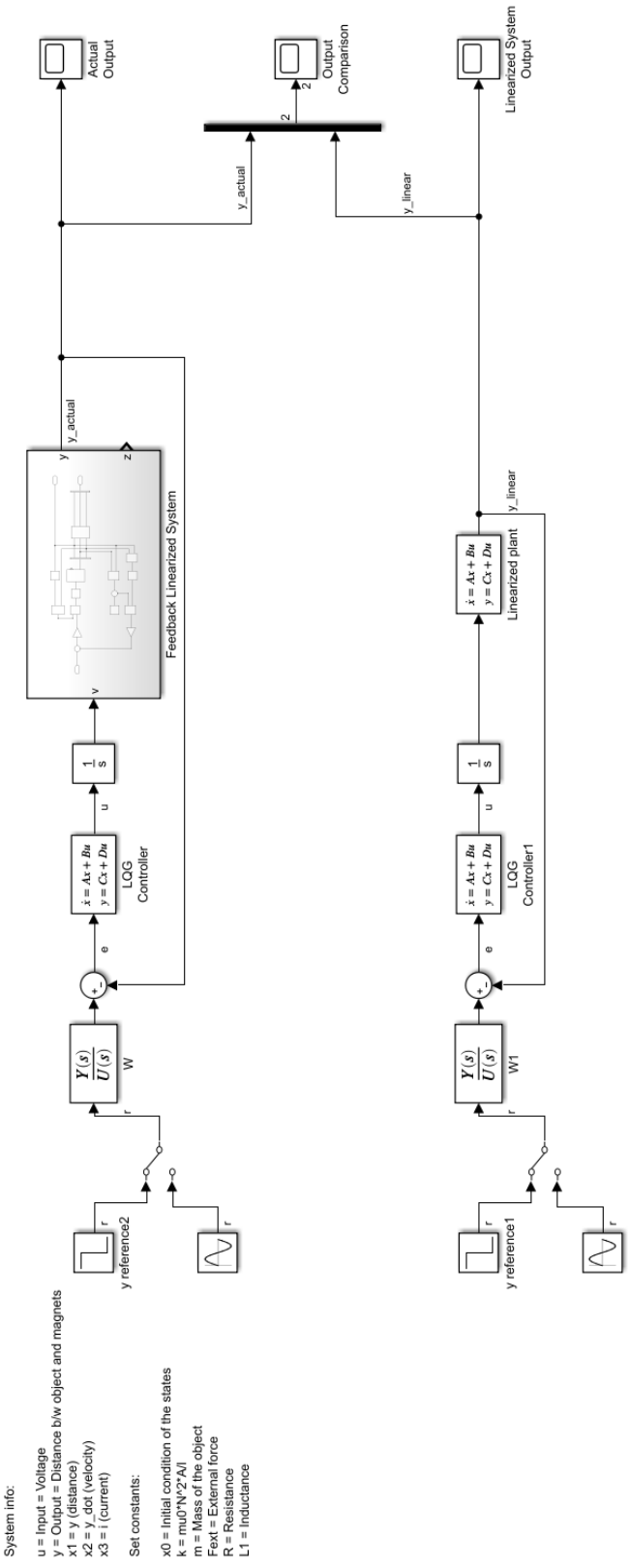

Figure 5.12: Feedback Linearized Nonlinear System with LQG Controller

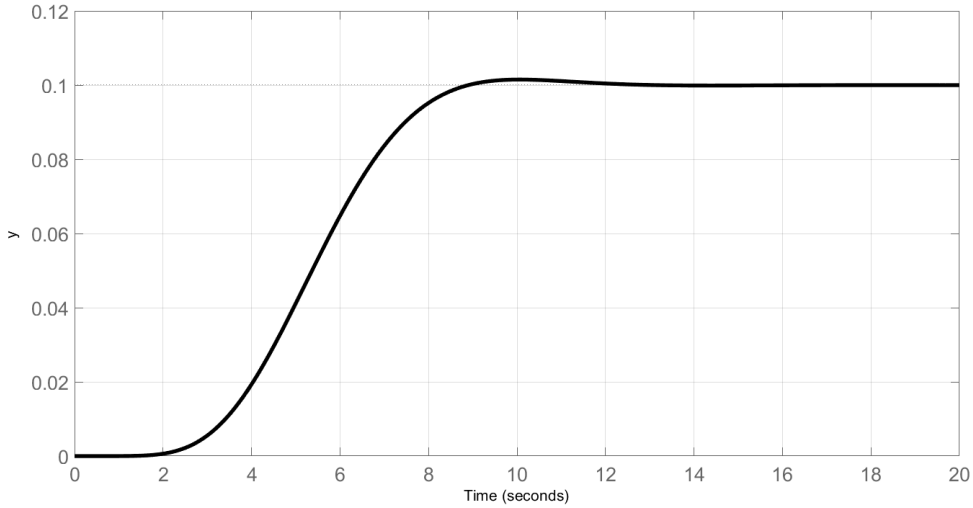

Figure 5.13: Feedback Linearized Closed Loop System Theoretical Step Response

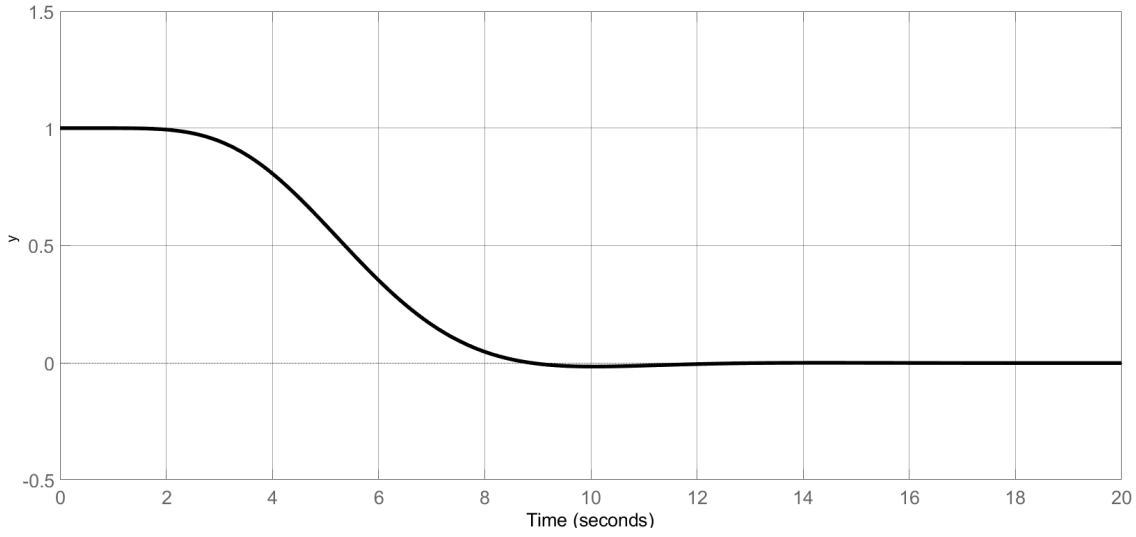

Figure 5.14: Feedback Linearized Closed Loop System Theoretical Output

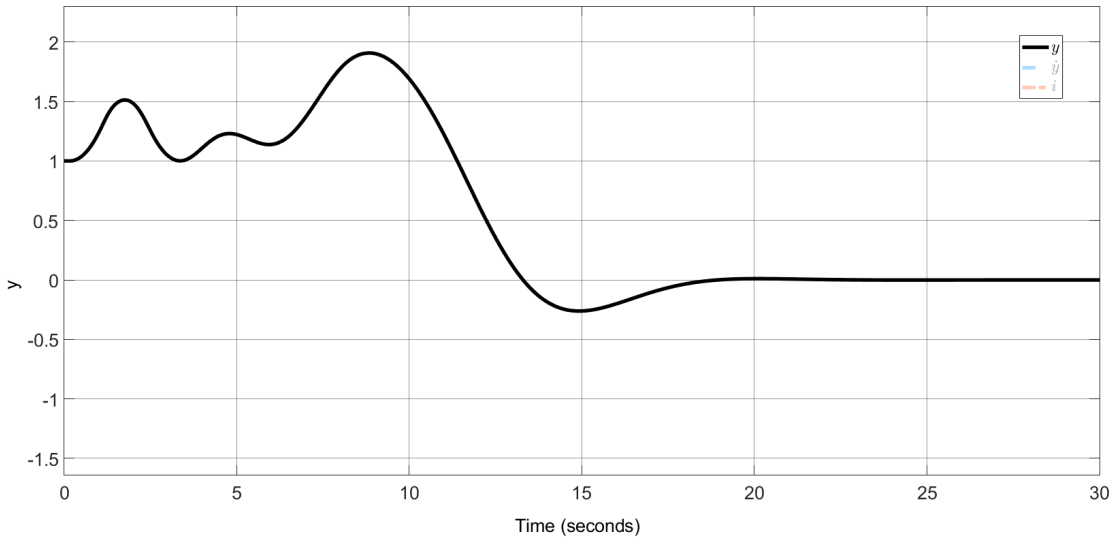

Figure 5.15: Feedback Linearized Closed Loop System Actual Output

Figure 5.13 shows the step response of the closed loop feedback linearized system with LQG controller. Figure 5.14 to Figure 5.16 show the step response of the feedback linearized system with an initial relative distance of $y = 1m$ between the satellites and how the LQG controller docks the two satellites. Figure 5.14 shows theoretically how the closed loop system is intended to behave, while Figure 5.15 shows the actual system output. A comparison can be found in Figure 5.16, with a comparison of the states in Figure 5.17.

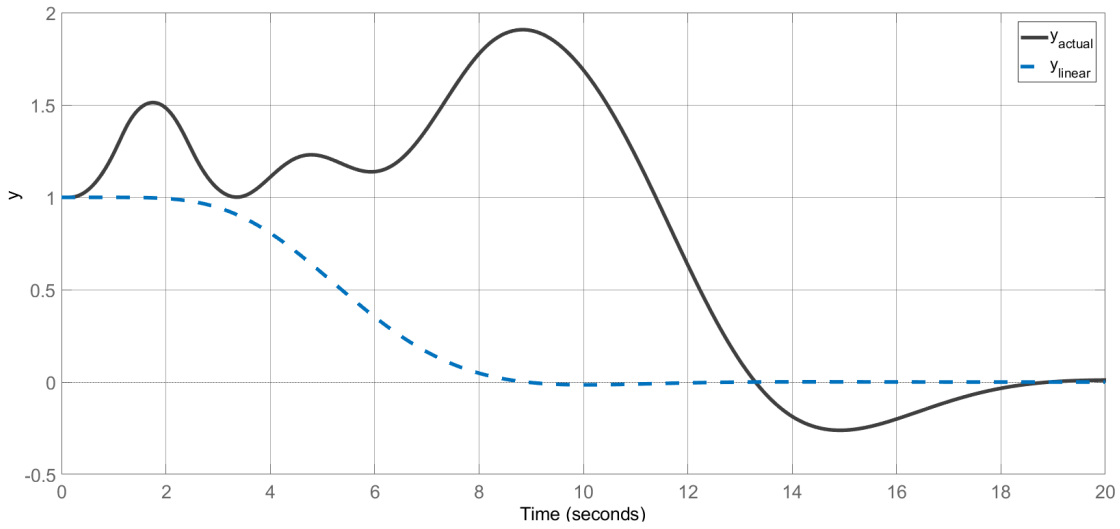

Figure 5.16: Feedback Linearized Closed Loop System Output Comparison

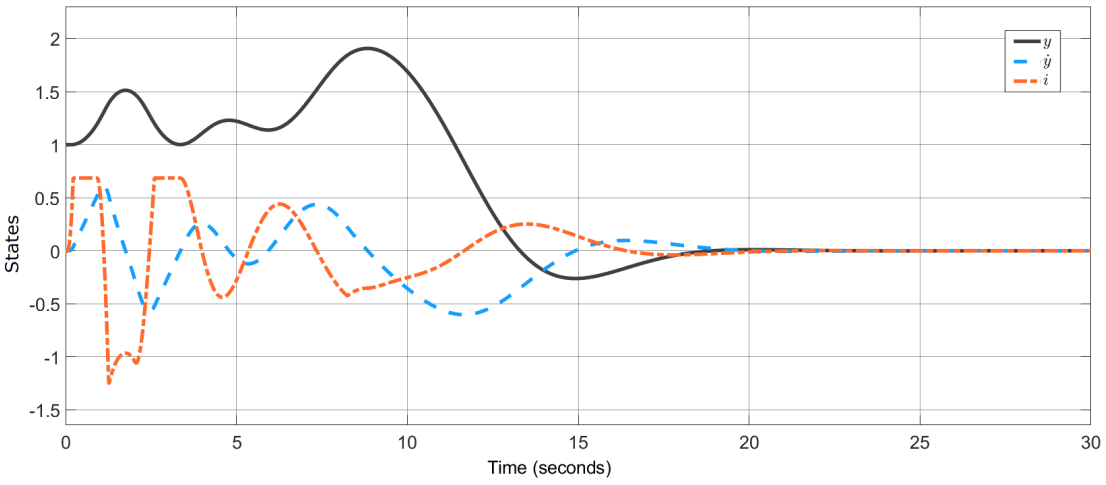

Figure 5.17: Feedback Linearized Closed Loop System Actual States

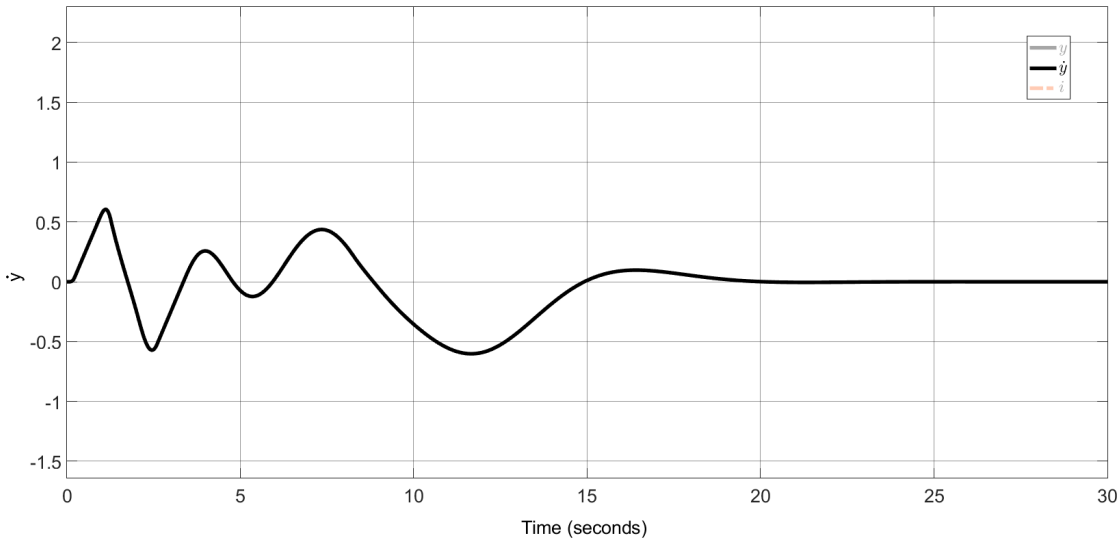

Figure 5.18: Feedback Linearized Closed Loop System Actual State $\dot{y}$

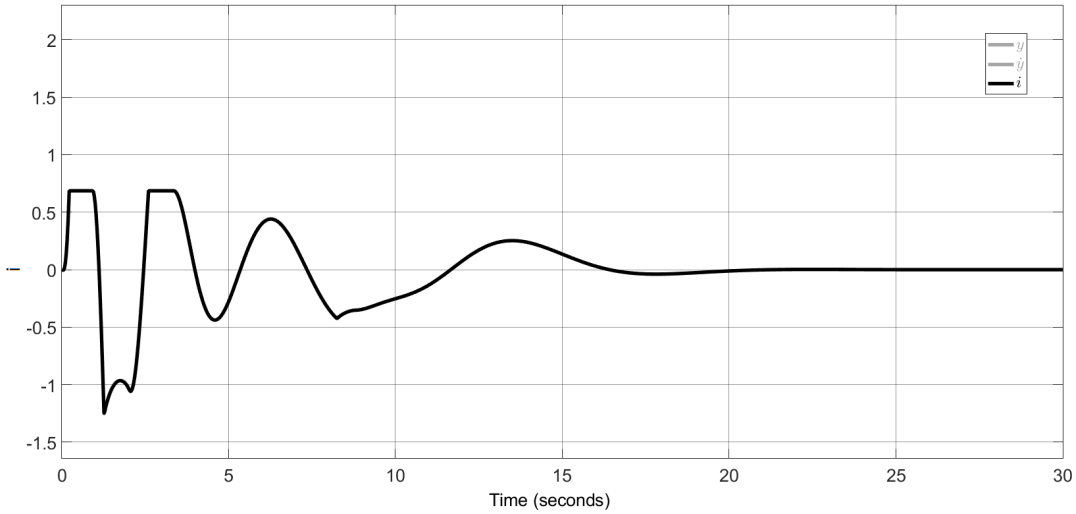

Figure 5.19: Feedback Linearized Closed Loop System Actual State i

5.2 Simulation

This section shows the results of the orbital simulation. Three types of results, a 3d simulation of the satellites going around the Earth, a close-up ground trace view

of the docking system in action, and the ground trace of the satellites are shown. Satellite A, which has the probe part of the docking system is represented by a red star marker with a red tail indicating its path history. Satellite B, which has the cone part of the docking system is represented by a cyan square marker with a cyan tail indicating its path. It is important to note that the cyan tail is not visible as the satellites are shown after the docking is performed. Figure 5.20, Figure 5.21, and Figure 5.22 indicate the position of the satellites at arbitrary time samples.

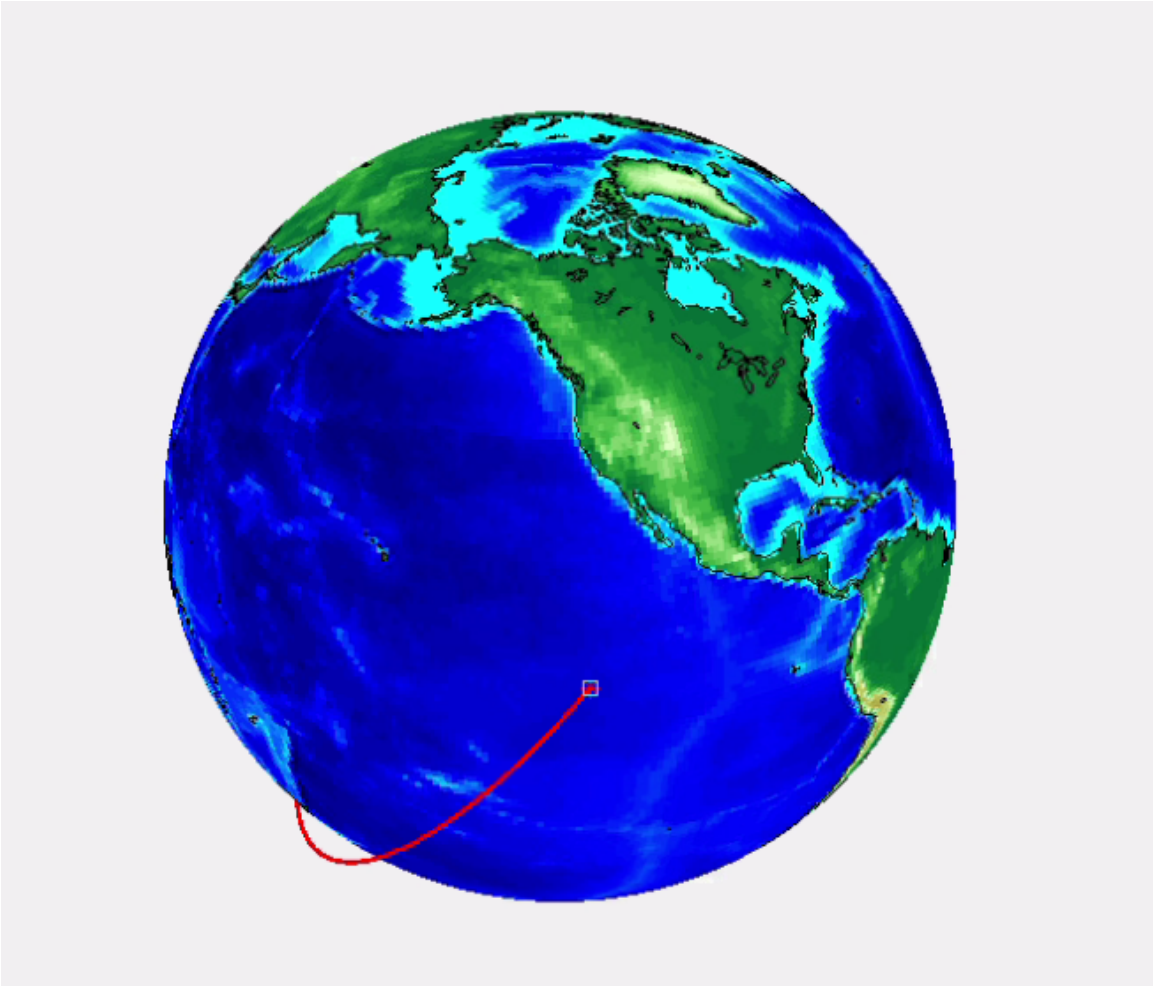

Figure 5.20: Satellite in Orbit at Time t1

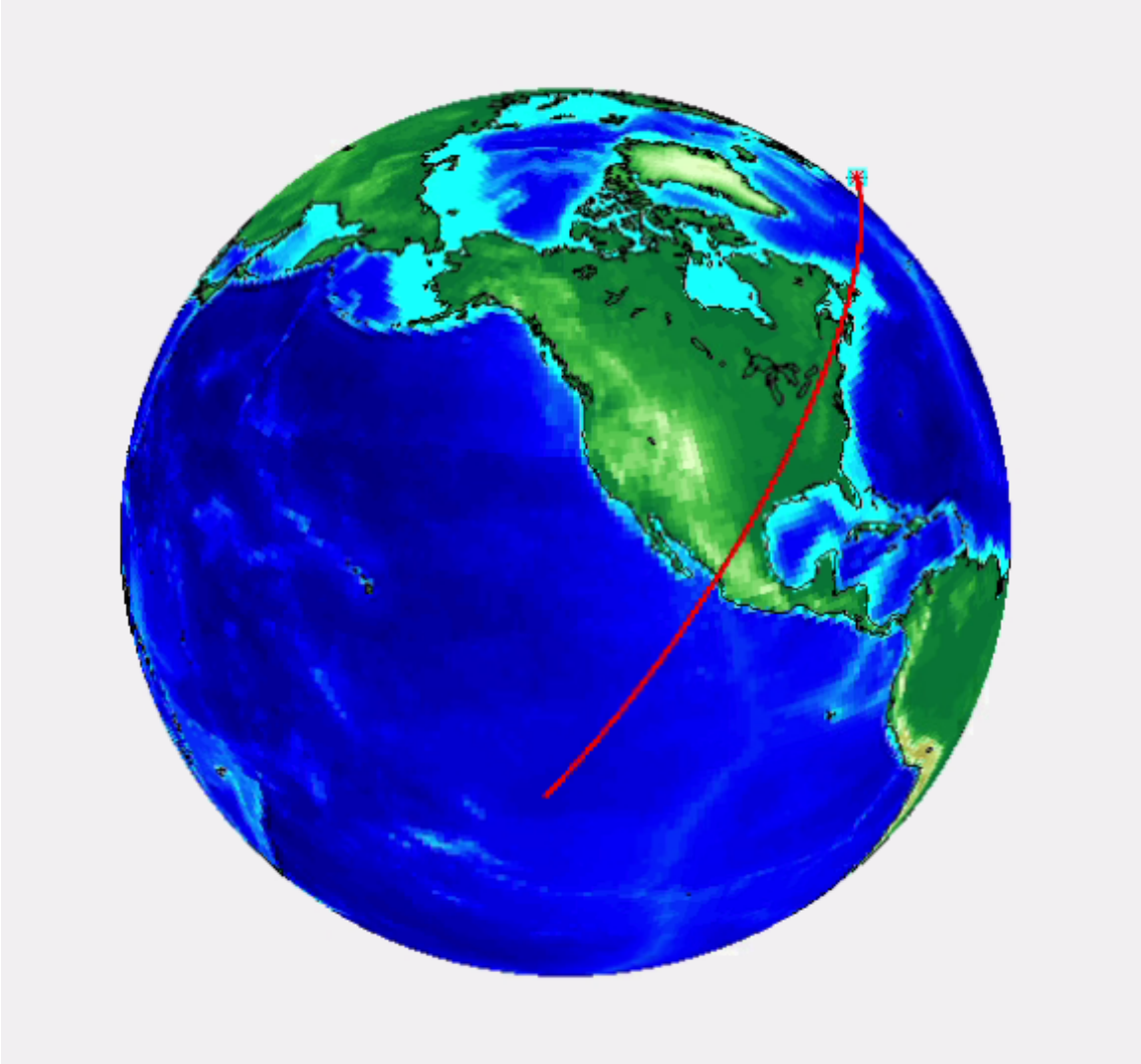

Figure 5.21: Satellite in Orbit at Time t2

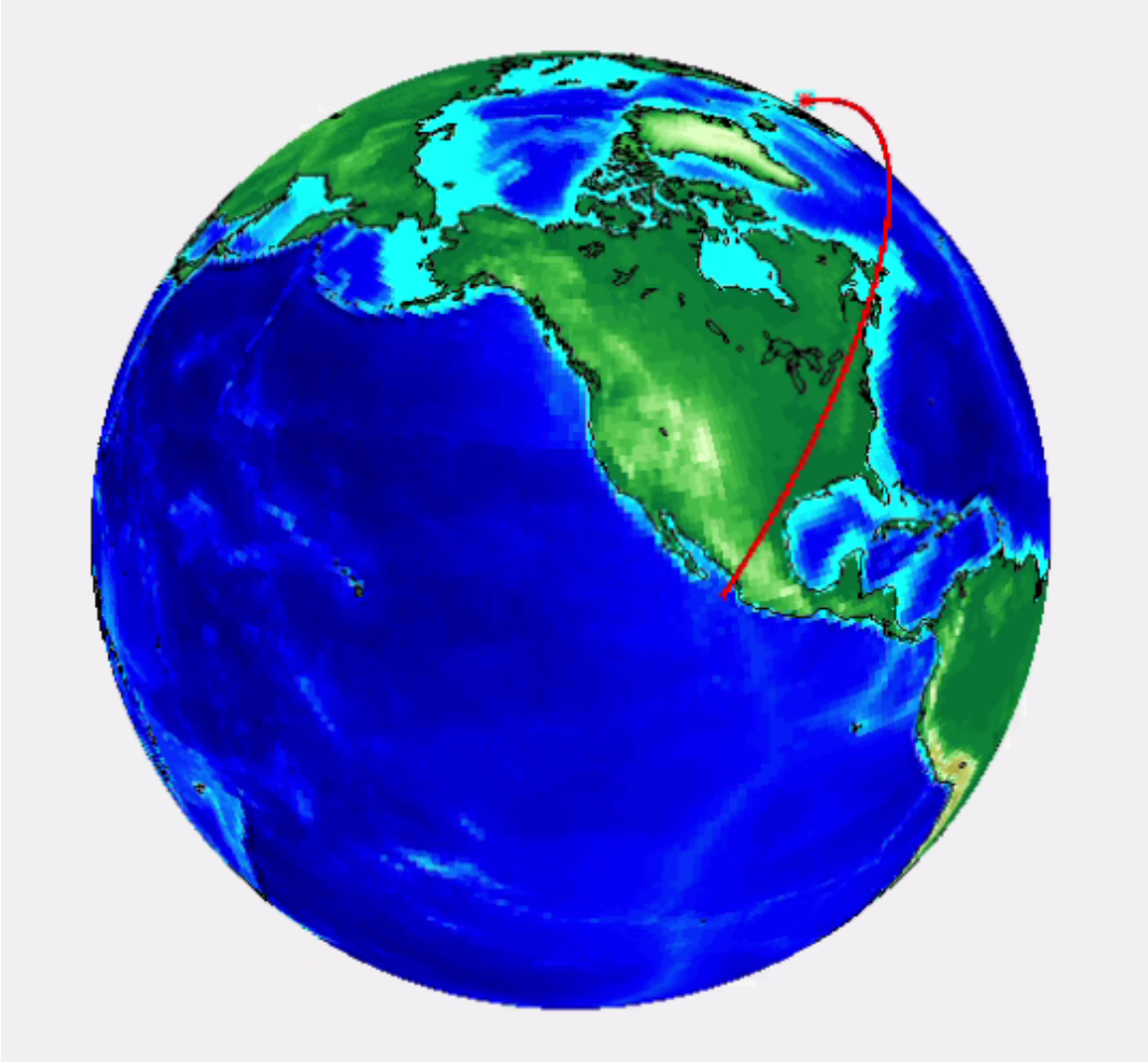

Figure 5.22: Satellite in Orbit at Time t3

Figure 5.23 to Figure 5.28 shows the actual docking progress. These figures show a top view of the satellites projected onto the Earth. Hence, this view can be considered as a close-up ground trace of the satellites. Satellite A follows the same step response pattern as shown in Figure 5.15. Satellite A starts out at $1m$ from satellite B, and moves away to a distance of approximately $2m$ before closing down to dock ($0m$). The relative distance Δy is indicated on the bottom left corner of every figure. It was found that the force while docking was as low as $1.15 \times 10^{-5} N$.

Figure 5.23: Docking of the Satellites in Orbit at Time $t_{dock}1$

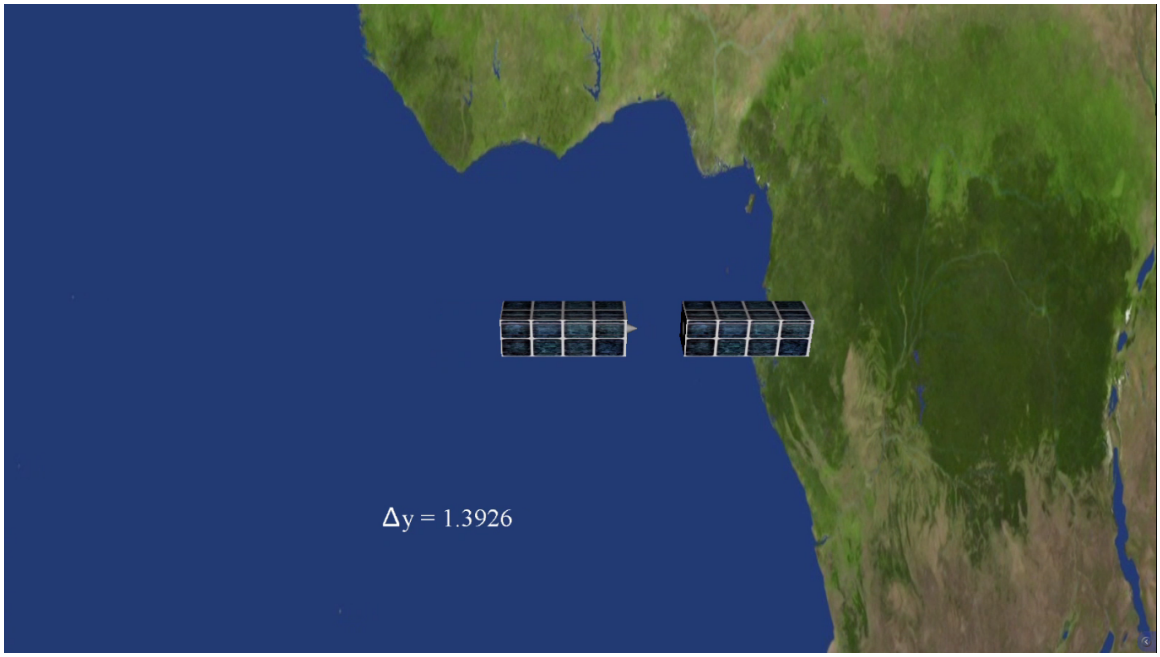

Figure 5.24: Docking of the Satellites in Orbit at Time $t_{dock}2$

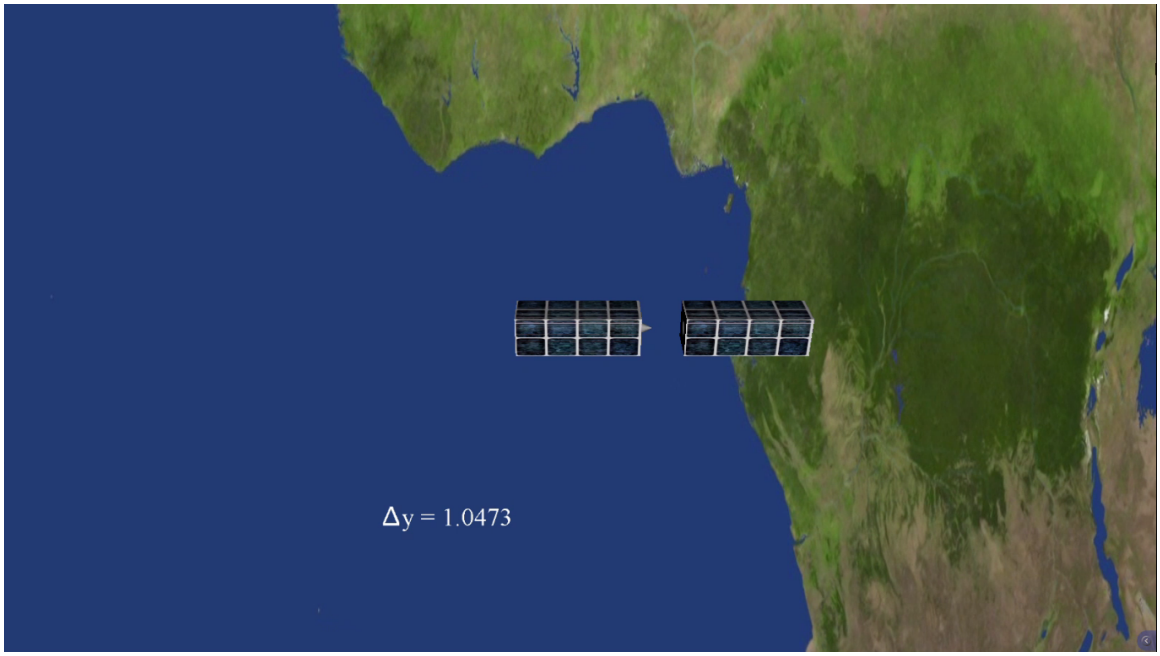

Figure 5.25: Docking of the Satellites in Orbit at Time $t_{dock}3$

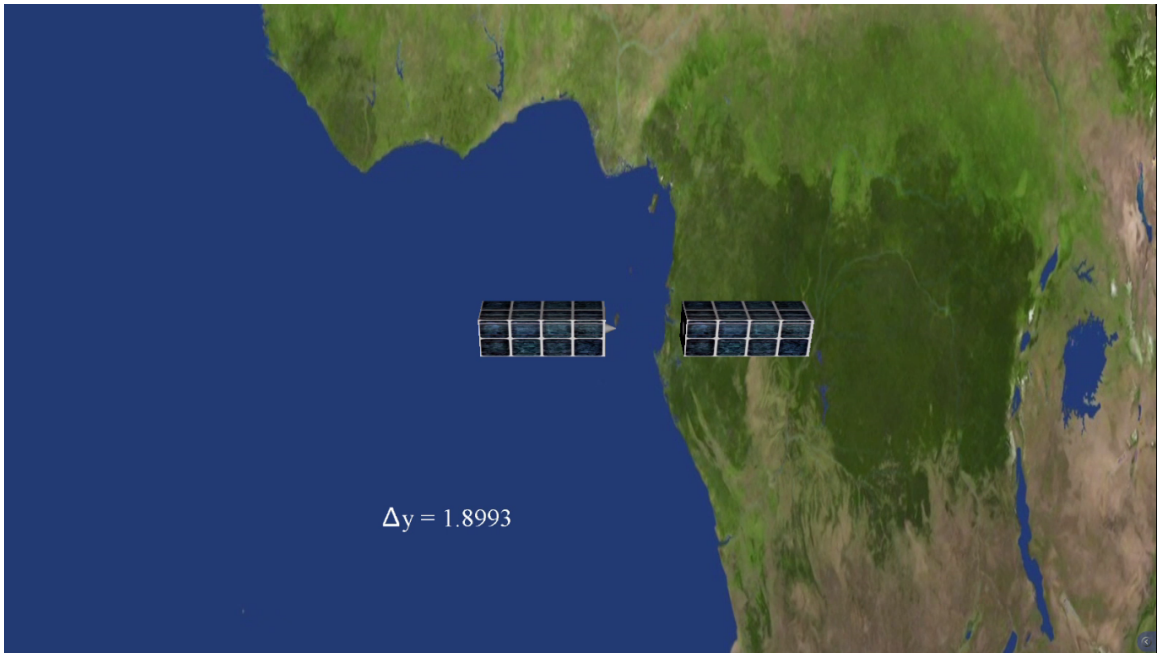

Figure 5.26: Docking of the Satellites in Orbit at Time $t_{dock}4$

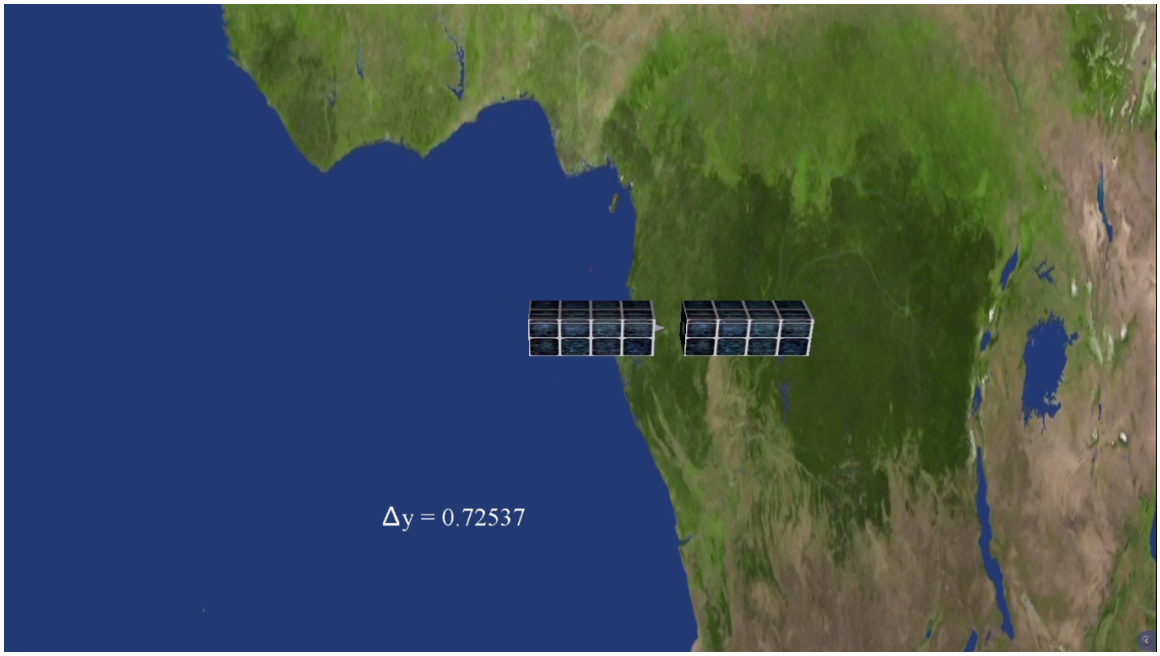

Figure 5.27: Docking of the Satellites in Orbit at Time $t_{dock}5$

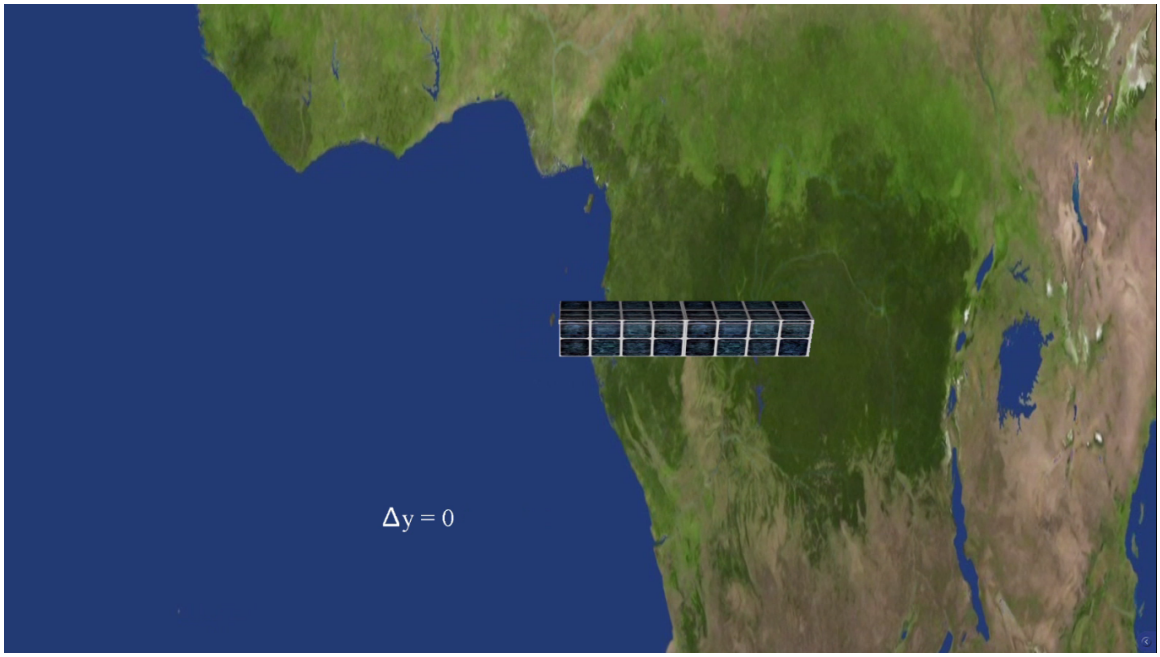

Figure 5.28: Docking of the Satellites in Orbit at Time $t_{dock}6$

Figure 5.29 ,Figure 5.30 , and Figure 5.31 show the ground trace of the satellites at arbitrary time samples after docking, with the red tail indicating the path history of the docked satellites.

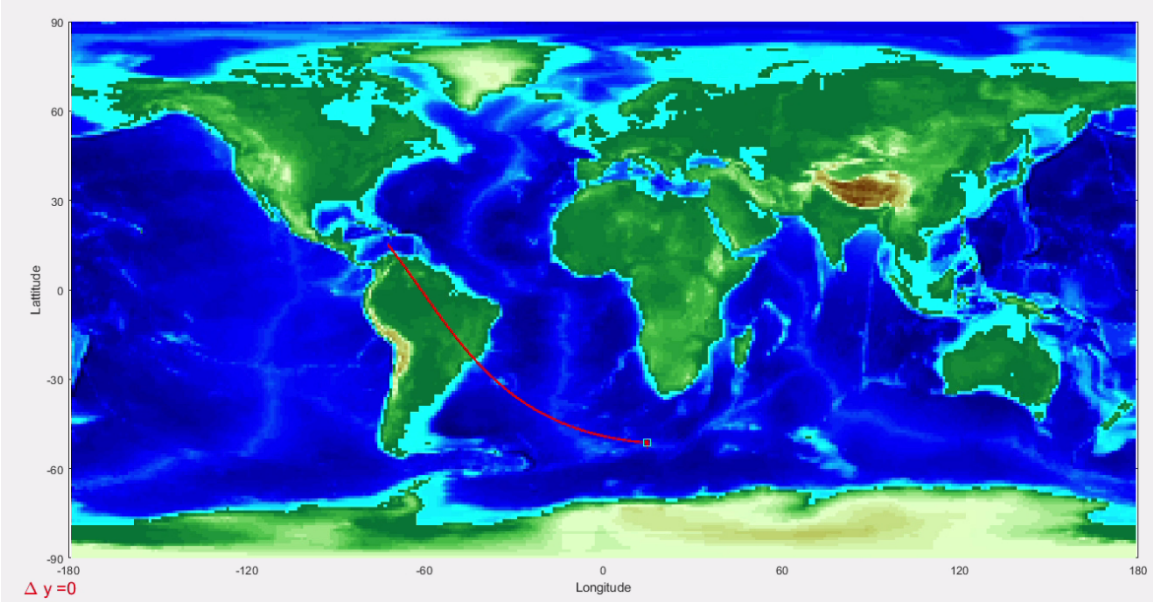

Figure 5.29: Satellite in Orbit at Time t4

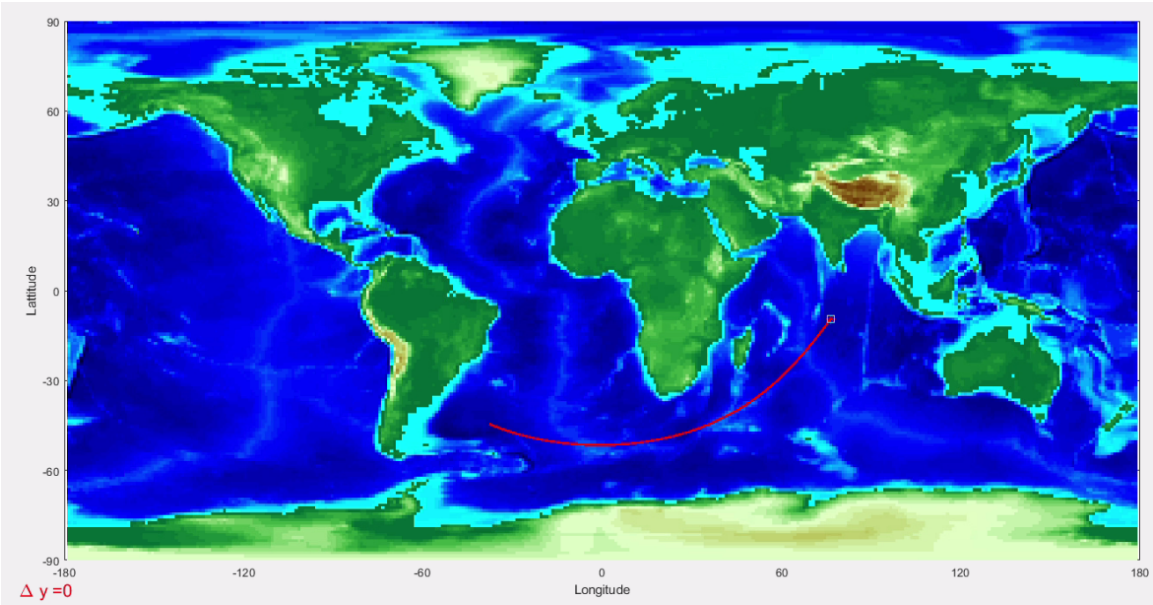

Figure 5.30: Satellite in Orbit at Time t5

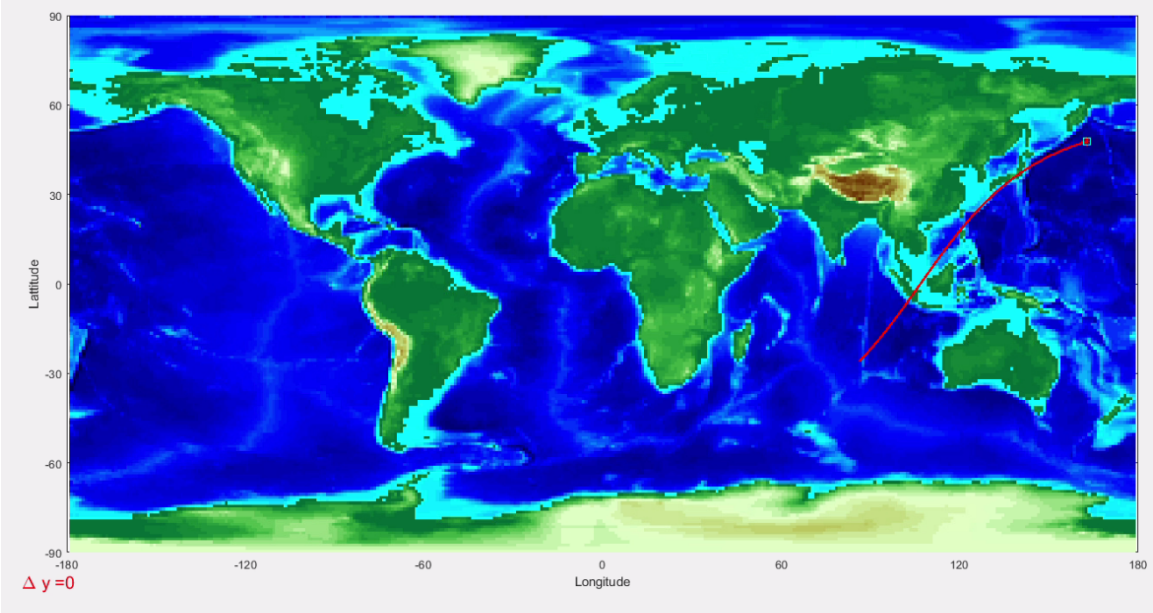

Figure 5.31: Satellite in Orbit at Time t6

5.3 Discussion on the Results

Some key results related to the electromagnetic docking system modeling, linearization of the system and integration with an orbit propagator were presented in this chapter. We saw that neither the controller designs based on bandwidth and robustness, nor the PID controller design could stabilize the Taylor series linearized system. Various bandwidth parameters were tested out, ranging from 0.01 $\frac{rad}{s}$ to 10^5 $\frac{rad}{s}$ for the former, and both Ziegler-Nichols methods for PID tuning for the latter. None of these designs could stabilize the system due to the subtle changes in bandwidth and phase margin which affected the system. This can be seen in the response of the LQR controller design, the exact bandwidth and phase margin required range required for stabilizing the system. However, when the LQG controller was implemented on the actual system, it failed. This is because the Taylor series linearization assumes that the system states lie close to the equilibrium states, and the

high degree of nonlinearity of the system makes it move away from the equilibrium states.

In the case of feedback linearization, the LQG controller is successful in controlling both the linearized system, as well as the actual nonlinear system, as feedback linearization is built into the resulting closed-loop system. The response of the resulting system deviates from the linearized system considerably, even after including the initial condition of the controller, removing the delay. This is because, the LQG controller designed for a feedback linearized system will be of a standard controllable canonical form, which does not model the type of nonlinearity present in the system. This nonlinearity is however transformed into a nonlinear input v. Hence, the deviation in the response of the system.

It is important to note that docking system is limited by the voltage capacity of the small satellites. Even the feedback linearized system is susceptible to errors. The reduce on the voltage saturation limit to say, 5V could make the system unstable for the same initial conditions. The main initial condition is the initial docking distance. It is shown that the controller design depends on the system parameters, and for a given set of parameters, the controller has a certain maximum initial distance it can reduce. Hence, this limit will change with the system parameters and the voltage saturation limits. Despite these limitations, the results show that it is possible to perform fine docking of small satellites with an electromagnetic docking system purely by feedback linearization and designing a linear controller like the LQG, without the bulky sensors like cameras, while producing very low docking forces of the order of $10^{-5}N$.

Chapter 6

CONCLUSION AND FUTURE WORK

Docking mechanisms not only enable assembly of large space structures, but also in repair. The current docking systems like the PDGF are costly and big. On top of that, they are operated by humans who are prone to errors. This thesis work on small satellite electromagnetic docking system ensures that docking mechanisms are smaller, cost effective, while being autonomous. Docking of these systems need to be fine, therefore an electromagnetic docking mechanism was considered. Inspiration was drawn from the electromagnetic levitation system and a model for the docking system was derived from first principles. This electromagnetic docking system is highly nonlinear in nature and using a single camera in the feedback loop to control the fine docking is prone to failure and is inefficient. Introducing multiple cameras will increase the system complexity and therefore the system efficiency. Hence, various control strategies without the camera in the loop were discussed. To control this system, two linearization techniques, namely Taylor Series Linearization and Feedback Linearization were performed. After Taylor Series linearization, various linear controller design methods like Bandwidth and Robustness design, PID controller design using Ziegler-Nichols tuning, and LQG design were discussed. It was concluded by the step responses of the systems that the closed loop system will be unstable as there is a large magnitude of deviation from the equilibrium states to the actual system states. Hence, Feedback Linearization was discussed in detail for the system, particularly Input-Output Linearization where the system is linearized from input to output. After feedback linearization, an LQG controller was designed to control the system. Finally, this system was integrated with an orbit propagator and a simula-

tion of the docking system was generated. Appropriate results related to the docking system modeling, control and simulation were shown and discussed in detail.

It is worth emphasizing that small satellite docking technology in general has not been tested in space and is still in the ground testing stage. Hence, a cubesat mission which can demonstrated this thesis work has been proposed and was discussed in fair detail. Supporting this, a hardware-in-the-loop testing of the fine docking mechanism would reinforce the results generated. Work is underway to perform hardware testing in order to advance this mission concept.

To conclude this, a reiteration of the capabilities this thesis work has been provided. The proposed docking system, enables assembly of large space structures with multiple small structures, eliminates humans from the loop by automating the docking process, and provides a fine docking controller which replaces cameras which are prone to failure.

REFERENCES

[1] B. D. Tapley and J. C. Ries, "Precision orbit determination for earth observation systems," *Encyclopedia of Space Science and Technology*, 2003.

[2] J. E. Krist and C. J. Burrows, "Phase-retrieval analysis of pre-and post-repair hubble space telescope images," *Applied optics*, vol. 34, no. 22, pp. 4951–4964, 1995.

[3] D. E. Hastings and C. Joppin, "On-orbit upgrade and repair: The hubble space telescope example," *Journal of spacecraft and rockets*, vol. 43, no. 3, pp. 614–625, 2006.

[4] E. W. Messerschmid and F. Renk, *Space stations*. Wiley Online Library, 2010.

[5] S. R. Ellis, "Collision in space," *Ergonomics in Design*, vol. 8, no. 1, pp. 4–9, 2000.

[6] J. Cook, V. Aksamentov, T. Hoffman, and W. Bruner, "Iss interface mechanisms and their heritage," in *AIAA SPACE 2011 conference & exposition*, 2011, p. 7150.

[7] C. Underwood, S. Pellegrino, V. J. Lappas, C. P. Bridges, and J. Baker, "Using cubesat/micro-satellite technology to demonstrate the autonomous assembly of a reconfigurable space telescope (aarest)," *Acta Astronautica*, vol. 114, pp. 112–122, 2015.

[8] S. Eckersley, C. Saunders, D. Lobb, G. Johnston, T. Baud, M. Sweeting, C. Underwood, C. Bridges, and R. Chen, "Future rendezvous and docking missions enabled by low-cost but safety compliant guidance navigation and control (gnc) architectures," in *Proceedings of The 15th Reinventing Space Conference*. British Interplanetary Society, 2017.

[9] J. Bowen, M. Villa, and A. Williams, "Cubesat based rendezvous, proximity operations, and docking in the cpod mission," 2015.

[10] J. Griesbach, J. Westphal, C. Roscoe, D. Hawes, and J. Carrico, "Proximity operations nano-satellite flight demonstration (ponsfd) rendezvous proximity operations design and trade studies," in *Advanced Maui Optical and Space Surveillance Technologies Conference*, 2013.

[11] L. Rodgers, N. Hoff, E. Jordan, M. Heiman, and D. Miller, "A universal interface for modular spacecraft," 2005.

[12] D. Miller, A. Saenz-Otero, J. Wertz, A. Chen, G. Berkowski, C. Brodel, S. Carlson, D. Carpenter, S. Chen, S. Cheng *et al.*, "Spheres: a testbed for long duration satellite formation flying in micro-gravity conditions," in *Proceedings of the AAS/AIAA Space Flight Mechanics Meeting, Clearwater, FL, Paper No. AAS 00-110*, 2000.

[13] M. Barbetta, A. Boesso, F. Branz, A. Carron, L. Olivieri, J. Prendin, G. Rodeghiero, F. Sansone, L. Savioli, F. Spinello *et al.*, "Arcade-r2 experiment on board bexus 17 stratospheric balloon," *CEAS Space Journal*, vol. 7, no. 3, pp. 347–358, 2015.

[14] J. Pei, L. Murchison, V. Stewart, J. Rosenthal, D. Sellers, M. Banchy, A. Ben-Shabat, R. Elandt, D. Elliott, and A. K. Weber, "Autonomous rendezvous and docking of two 3u cubesats using a novel permanent-magnet docking mechanism," in *54th AIAA Aerospace Sciences Meeting*, 2016, p. 1465.

[15] D. W. Miller, S. Mohan, and J. Budinoff, "Assembly of a large modular optical telescope (almost)," in *Space Telescopes and Instrumentation 2008: Optical, Infrared, and Millimeter*, vol. 7010. International Society for Optics and Photonics, 2008, p. 70102H.

[16] R. McCormick, A. Austin, L. Cubrich, B. Marth, R. Mukherjee, T. Wenger, M. Patel, and K. Ho, "Development of miniature robotic manipulators to enable smallsat clusters," in *Aerospace Conference, 2017 IEEE*. IEEE, 2017, pp. 1–15.

[17] D. Ye, Z. Yuan, L. Wen-juan, and T. Wen-ming, "Dynamic performance analysis of capture and separation process for a microsatellite docking device," *International Journal of Future Generation Communication and Networking*, vol. 8, no. 3, pp. 283–290, 2015.

[18] X. Zhang, Y. Huang, X. Chen, and W. Han, "Modeling of a space flexible probe–cone docking system based on the kane method," *Chinese Journal of Aeronautics*, vol. 27, no. 2, pp. 248–258, 2014.

[19] Y. Qin, H. Peng, W. Ruan, J. Wu, and J. Gao, "A modeling and control approach to magnetic levitation system based on state-dependent arx model," *Journal of Process Control*, vol. 24, no. 1, pp. 93–112, 2014.

[20] R. V. Gandhi and D. M. Adhyaru, "Feedback linearization based optimal controller design for electromagnetic levitation system," in *Control, Instrumentation, Communication and Computational Technologies (ICCICCT), 2016 International Conference on*. IEEE, 2016, pp. 36–41.

[21] A. Romero Acero, J. A. Orozco Quiceno, J. Bulies, and J. Alberto, "Modelling and simulation of lqr and lfsv controllers in the magnetic levitation system (mls)," *Prospectiva*, vol. 14, no. 1, pp. 28–38, 2016.

[22] W. J. Larson and J. R. Wertz, "Space mission analysis and design," Microcosm, Inc., Torrance, CA (US), Tech. Rep., 1992.

[23] R. Steven Nerem, "Earth orbiting satellite theory," *Van Nostrand's Scientific Encyclopedia*, 2006.

[24] V. A. Chobotov, "Spacecraft attitude dynamics and control," *NASA STI/Recon Technical Report A*, vol. 92, 1991.

[25] R. T. Nallapu, R. Furfaro, A. Ravindran, E. Asphaug, H. Kalita, J. Thangavelautham, and V. Reddy, "Smart camera system on-board a cubesat for space-based object reentry and tracking," 2018.

[26] R. C. Dorf and R. H. Bishop, *Modern control systems*. Pearson, 2011.

[27] M. A. Henson and D. E. Seborg, *Nonlinear process control*. Prentice Hall PTR Upper Saddle River, New Jersey, 1997.